

# Sea Ice Changes in the Southwest Pacific Sector of the Southern Ocean During the Last 140,000 Years

Jacob Jones<sup>1</sup>, Karen E Kohfeld<sup>1,2</sup>, Helen Bostock<sup>3,4</sup>, Xavier Crosta<sup>5</sup>, Melanie Liston<sup>6</sup>, Gavin Dunbar<sup>6</sup>, Zanna Chase<sup>7</sup>, Amy Leventer<sup>8</sup>, Harris Anderson<sup>7</sup>, Geraldine Jacobsen<sup>9</sup>

<sup>1</sup> School of Resource and Environmental Management, Simon Fraser University, Burnaby, Canada

<sup>2</sup> School of Environmental Science, Simon Fraser University, Burnaby, Canada

<sup>3</sup> School of Earth and Environmental Sciences, The University of Queensland, Brisbane, Australia

<sup>4</sup> National Institute of Water and Atmospheric Research (NIWA), Wellington, New Zealand

<sup>5</sup> Université de Bordeaux, CNRS, EPHE, UMR 5805 EPOC, Pessac, France

<sup>6</sup> Antarctic Research Centre, Victoria University of Wellington, Wellington, New Zealand

<sup>7</sup> Institute of Marine and Antarctic Studies, University of Tasmania, Hobart, Australia

<sup>8</sup> Geology Department, Colgate University, Hamilton, NY, USA

<sup>9</sup> Centre for Accelerator Science, Australian Nuclear Science and Technology Organisation, Lucas Heights, NSW, Australia

Correspondence to: Jacob Jones (jacob\_jones@sfu.ca)

## Abstract

Sea ice expansion in the Southern Ocean is believed to have contributed to glacial-interglacial atmospheric CO<sub>2</sub> variability by inhibiting air-sea gas exchange and influencing the ocean's meridional overturning circulation. However, limited data on past sea ice coverage over the last 140 ka (a complete glacial cycle) have hindered our ability to link sea ice expansion to oceanic processes that affect atmospheric CO<sub>2</sub> concentration. Assessments of past sea ice coverage using diatom assemblages have primarily focused on the Last Glacial Maximum (~21 ka BP) to Holocene, with few quantitative reconstructions extending to the onset of glacial Termination II (~135 ka BP). Here we provide new estimates of winter sea ice concentrations (WSIC) and summer sea surface temperatures (SSST) for a full glacial-interglacial cycle from the southwestern Pacific sector of the Southern Ocean using the Modern Analog Technique (MAT) on fossil diatom assemblages from deep-sea core TAN1302-96. We examine how the timing of changes in sea ice coverage relates to ocean circulation changes and previously proposed mechanisms of early glacial CO<sub>2</sub> drawdown. We then place SSST estimates within the context of regional SSST records to better understand how these surface temperature changes may be influencing oceanic CO<sub>2</sub> uptake. We find that winter sea ice was absent over the core site during the early glacial period until MIS 4 (~65 ka BP), suggesting that sea ice may not have been a major contributor to early-glacial CO<sub>2</sub> drawdown. Sea ice expansion throughout the glacial-interglacial cycle, however, appears to coincide with observed regional reductions in Antarctic Intermediate Water production and subduction, suggesting that sea ice may have influenced intermediate ocean circulation changes. We observe an early glacial (MIS 5d) weakening of meridional SST gradients between 42° to 59°S throughout the region, which may have contributed to early reductions in atmospheric CO<sub>2</sub> concentrations through its impact on air-sea gas exchange.

Deleted: Australian Nuclear Science and Technology (ANSTO), Lucas Heights, New South Wales, Australia

Deleted:

Deleted: w

Deleted: sSST

Deleted: s

Deleted: -

Deleted: changes

Deleted: s

Formatted: Subscript

Deleted: ,

Deleted: and

Deleted: w

Deleted: the

Deleted: changes

Deleted: .

Deleted: (59.09°S, 157.05°E, water depth 3099 m).

Deleted: consolidated over the core site during the latter part of the penultimate glaciation, Marine Isotope Stage (MIS) 6 (from at least 140 to 134 ka), when sSSTs were between ~1 and 1.5°C. The winter sea ice edge then retreated rapidly as sSSTs increased during the transition into the Last Interglacial Period (MIS 5e), reaching ~4.5°C by 125 ka. As the Earth entered the early glacial stages, sSSTs began to decline around 112 ka, but winter sea ice largely remained absent until ~65 ka during MIS 4, when it was sporadically present but unconsolidated (<40% WSIC). WSIC and sSSTs reached their maximum concentration and coolest values by 24.5 ka, just prior to the Last Glacial Maximum. Winter sea ice remained absent throughout the Holocene, while sSSTs briefly exceeded modern values, reaching ~5°C by 11.4 ka, before decreasing to ~4°C and stabilizing. The

Deleted: ce

Deleted: of sea ice coverage

Formatted: Subscript

Deleted: s

Deleted: at this time

Deleted: During MIS 5d,

Deleted: We observe we observe an early glacial (MIS 5d) weakening of meridional SST gradients between 42° to 59°S throughout the region, which may have contributed to early reductions in atmospheric CO<sub>2</sub> concentrations through its impact on air-sea gas exchange.

Deleted: during MIS 4

Deleted: s

85

## 86 1.0 Introduction

87 Antarctic sea ice has been suggested to have played a key role in glacial-interglacial  
88 atmospheric CO<sub>2</sub> variability (e.g., Stephens & Keeling, 2000; Ferrari et al., 2014; Kohfeld &  
89 Chase, 2017; Stein et al., 2020). Sea ice has been dynamically linked to several processes that  
90 promote deep ocean carbon sequestration, namely by: [1] reducing deep ocean outgassing by  
91 ice-induced ‘capping’ and surface water stratification (Stephens & Keeling, 2000; Rutgers van  
92 der Loeff et al., 2014), and [2] influencing ocean circulation through water mass formation and  
93 deep-sea stratification, leading to reduced diapycnal mixing and reduced CO<sub>2</sub> exchange  
94 between the surface and deep ocean (Toggweiler, 1999; Bouttes et al., 2010; Ferrari et al.,  
95 2014). Numerical modelling studies have shown that sea ice-induced capping, stratification, and  
96 reduced vertical mixing may be able to account for a significant portion of the total CO<sub>2</sub>  
97 variability on glacial-interglacial timescales (between 40-80 ppm) (Stephens & Keeling, 2000;  
98 Galbraith & de Lavergne, 2018; Marzocchi & Jansen, 2019; Stein et al., 2020). However, debate  
99 continues surrounding the timing and magnitude of sea ice impacts on glacial-scale carbon  
100 sequestration (e.g., Morales Maqueda & Rahmstorf, 2002; Archer et al., 2003; Sun &  
101 Matsumoto, 2010; Kohfeld & Chase, 2017).

102 Past Antarctic sea ice coverage has been estimated primarily through diatom-based  
103 reconstructions, with most work focusing on the Last Glacial Maximum (LGM), specifically the  
104 EPILOG timeslice as outlined in Mix et al. (2001), corresponding to 23 to 19 thousand years ago  
105 (ka) before present (BP). During the LGM, these reconstructions suggest that winter sea ice  
106 expanded by 7-10° latitude (depending on the sector of the Southern Ocean), which  
107 corresponds to substantial expansion of total winter sea ice coverage compared to modern  
108 observations (Gersonde et al., 2005; Benz et al., 2016; Lhardy et al., 2021). Currently, only a  
109 handful of studies provide quantitative sea-ice coverage estimates back to the penultimate  
110 glaciation, Marine Isotope Stage (MIS) 6 (~194 to 135 ka BP) (Gersonde & Zielinski, 2000; Crosta  
111 et al., 2004; Schneider-Mor et al., 2012; Esper & Gersonde 2014a; Ghadi et al. 2020). These  
112 studies primarily cover the Atlantic sector, with only one published sea ice record from each of  
113 the Indian (SK200-33 from Ghadi et al., 2020), eastern Pacific (PS58/271-1 from Esper &

Deleted: an approximate doubling

Deleted:

116 Gersonde, 2014a), and southwestern Pacific sectors (SO136-111 from Crosta et al., 2004).  
117 These glacial-interglacial sea ice records show heterogeneity between sectors in both timing  
118 and coverage. While the Antarctic Zone (AZ) in the Atlantic sector experienced early sea ice  
119 advance corresponding to MIS 5d cooling (i.e., 115 to 105 ka BP) (Gersonde & Zielinski, 2000;  
120 Bianchi & Gersonde, 2002; Esper & Gersonde, 2014a), the Indian and Pacific sector cores in the  
121 AZ show only minor sea ice advances during this time (Crosta et al., 2004; Ghadi et al., 2020).  
122 The lack of spatial and temporal resolution has resulted in significant uncertainty in our ability  
123 to evaluate the timing and magnitude of sea ice change during a full glacial cycle across the  
124 Southern Ocean, and to link sea ice to glacial-interglacial CO<sub>2</sub> variability.

125 This paper provides new winter sea ice concentration (WSIC) and summer sea surface  
126 temperature (SSST) estimates for the southwestern Pacific sector of the Southern Ocean over  
127 the last 140 ka BP. WSIC, which is a grid-scale observation of the mean state fraction of ocean  
128 area that is covered by sea ice over the sample period, and SSST estimates are produced by  
129 applying the Modern Analog Technique (MAT) to fossil diatom assemblages from sediment core  
130 TAN1302-96 (59.09°S, 157.05°E, water depth 3099 m). We place this record within the context  
131 of sea ice and SSST changes from the region using previously published records from SO136-111  
132 (56.66°S, 160.23°E, water depth 3912 m), which has recalculated WSIC and SSST estimates  
133 presented in this study, and nearby marine core E27-23 (59.61°S, 155.23°E; water depth 3182  
134 m) (Ferry et al., 2015). Using these records, we compare the timing of sea ice expansion to early  
135 glacial-interglacial CO<sub>2</sub> variability to test the hypothesis that the initial CO<sub>2</sub> drawdown (~115 to  
136 100 ka BP) resulted from reduced air-sea gas exchange in response to sea ice capping and  
137 surface water stratification (Kohfeld and Chase, 2017). We then consider alternative oceanic  
138 drivers of early atmospheric CO<sub>2</sub> variability and place our SSST estimates within the context of  
139 other studies to examine how regional cooling and a weakening in meridional SST gradients  
140 might affect air-sea disequilibrium and early CO<sub>2</sub> drawdown (Khatiwala et al., 2019). Finally, we  
141 compare our WSIC estimates with regional reconstructions of Antarctic Intermediate Water  
142 (AAIW) production and subduction variability using previously published carbon isotope  
143 analyses on benthic foraminifera from intermediate to deep-water depths in the southwest

Deleted: )

Deleted: wSIC

Deleted: sSST

Deleted: SSST

Deleted: s

Deleted: and wSIC are

Deleted: d

Deleted: sSST

Deleted: wSIC

Deleted: sSST

Deleted: ,

Deleted: sSST

Deleted: s

Deleted: wSIC

158 Pacific sector of the Southern Ocean, to test the hypothesis that sea ice expansion is  
159 dynamically linked to AAIW production and variability (Ronge et al., 2015).

160

## 161 2.0 Methods

### 162 2.1 Study Site and Age Determination

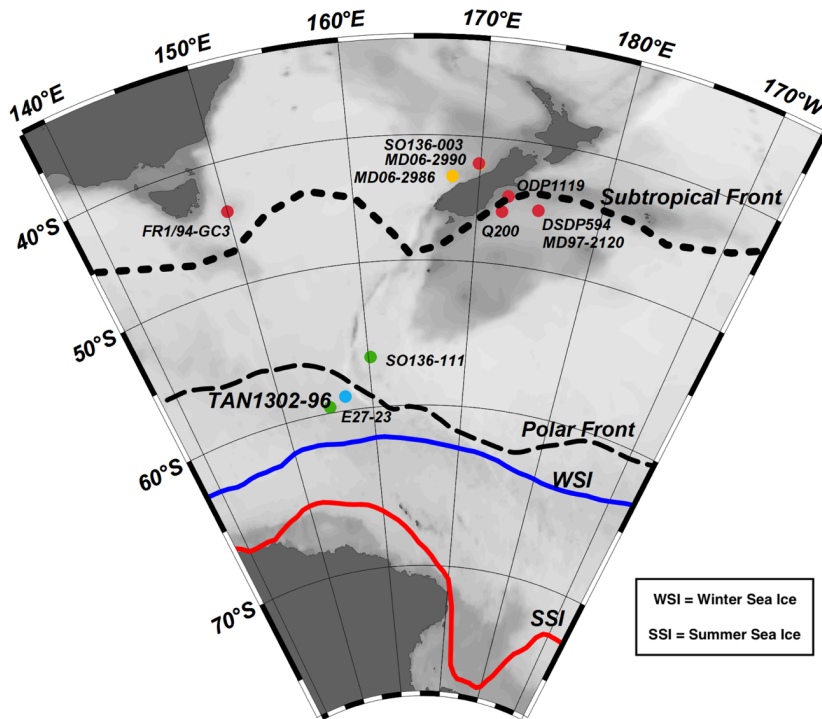
163 We reconstruct diatom-based ~~WSIC~~ and ~~SSST~~ using marine sediment core TAN1302-96  
164 (59.09°S, 157.05°E, water depth 3099 m) (Figure 1). The 364 cm core was collected in March  
165 2013 using a gravity corer during the return of the *RV Tangaroa* from the Mertz Polynya in  
166 Eastern Antarctica (Williams et al., 2013). The core is situated in the western Pacific sector of  
167 the Southern Ocean, on the southwestern side of the Macquarie Ridge, approximately 3-4°  
168 south of the average position of the Polar Front (PF) at 157°E (Sokolov & Rintoul, 2009).

Formatted: Line spacing: single

Deleted: &

Deleted: WSIC

Deleted: SSST



169

173 **Figure 1:** Map of the southwestern Pacific sector of the Southern Ocean including the study  
174 site, TAN1302-96 (blue circle), and additional **published** cores providing **sea-ice extent data**,  
175 SO136-111 and E27-23 (green circles), SST reconstructions (red circles), and  $\delta^{13}\text{C}$  of benthic  
176 foraminifera (yellow circles). **Note that some cores may not appear present in the figure**  
177 **because of their proximity to other cores.** Data for **all** cores are provided in Table 2. Dashed  
178 lines show the average location of the Subtropical and Polar Fronts (Smith et al., 2013; Bostock  
179 et al., 2015), **and** red and blue lines show **mean** positions of **modern** summer **sea ice (SSI)** and  
180 winter sea ice (**WSI**) extents, respectively (Reynolds et al., 2002; 2007).

- Deleted:
- Deleted: supporting information on sea ice extent
- Deleted: Metad
- Deleted: these
- Deleted: A1
- Deleted: approximate

182 The age model for TAN1302-96 (Figures 2 and 3) was based on a combination of  
183 radiocarbon dating of mixed foraminiferal assemblages and stable oxygen isotope stratigraphy  
184 on *Neogloboquadrina pachyderma* (180-250  $\mu\text{m}$ ). Seven accelerator mass spectrometry (AMS)  
185  $^{14}\text{C}$  samples were collected (Table A1 in Appendix A) and consisted of mixed assemblages of  
186 planktonic foraminifera (*N. pachyderma* and *Globigerina bulloides*,  $>250 \mu\text{m}$ ). Three of the  
187 seven radiocarbon samples (NZA 57105, 57109, and 61429) were previously published in  
188 Prebble et al. (2017), and four additional samples (OZX 517-520) were added to improve the  
189 dating reliability (Table A1 in Appendix A). OZX 519 and OZX 520 produced dates that were not  
190 distinguishable from background ( $>57.5 \text{ ka BP}$ ) and were subsequently excluded from the age  
191 model. The TAN1302-96 oxygen isotopes were run at the National Institute of Water and  
192 Atmospheric Research (NIWA) using the Kiel IV individual acid-on-sample device and analysed  
193 using Finnigan MAT 252 Mass Spectrometer. The precision is  $\pm 0.07\%$  for  $\delta^{18}\text{O}$  and  $\pm 0.05\%$  for  
194  $\delta^{13}\text{C}$ .

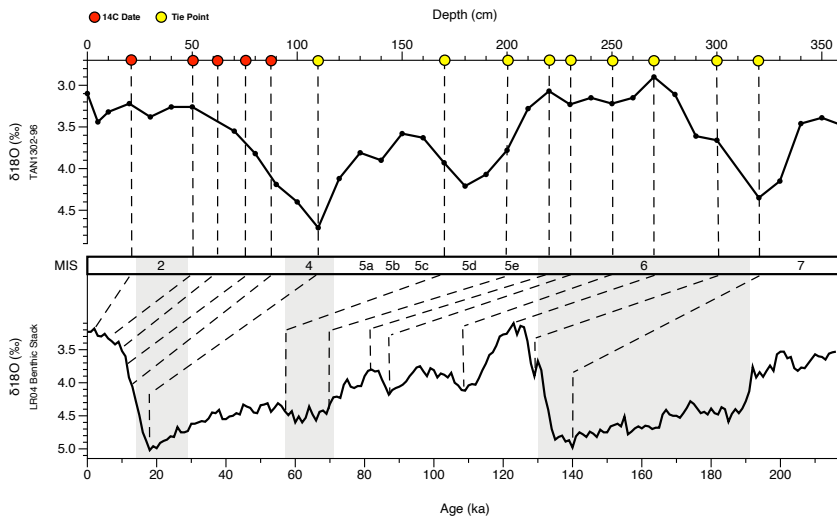
- Deleted: ,
- Deleted: e
- Deleted: ,

195 The age model was constructed using the 'Undatable' MATLAB software by  
196 bootstrapping at 10% and using an x-factor of 0.1 (Lougheed & Obrochta, 2019), which scales  
197 Gaussian distributions of sediment accumulation uncertainty (Table A2 in Appendix A). Below  
198 100 cm, **9** tie points were selected at positions of maximum change in  $\delta^{18}\text{O}$  and were correlated  
199 to the LR04 benthic stack (Lisiecki & Raymo, 2005) (Fig 2; Table A2 in Appendix A). **Uncertainty**  
200 **associated with stratigraphic correlation to the LR04 stack has been estimated to be  $\pm 4 \text{ ka}$**   
201 **(Lisiecki & Raymo, 2005).** We used a conservative marine reservoir age (MRA) for radiocarbon  
202 calibration of  $1000 \pm 100$  years, in line with regional estimates in Paterne et al. (2019) and  
203 modelled estimates by Butzin et al. (2017; 2020). The age model shows that TAN1302-96

- Deleted: six
- Formatted: Font: (Default) +Body (Calibri)
- Formatted: Font: (Default) +Body (Calibri)
- Deleted: 50

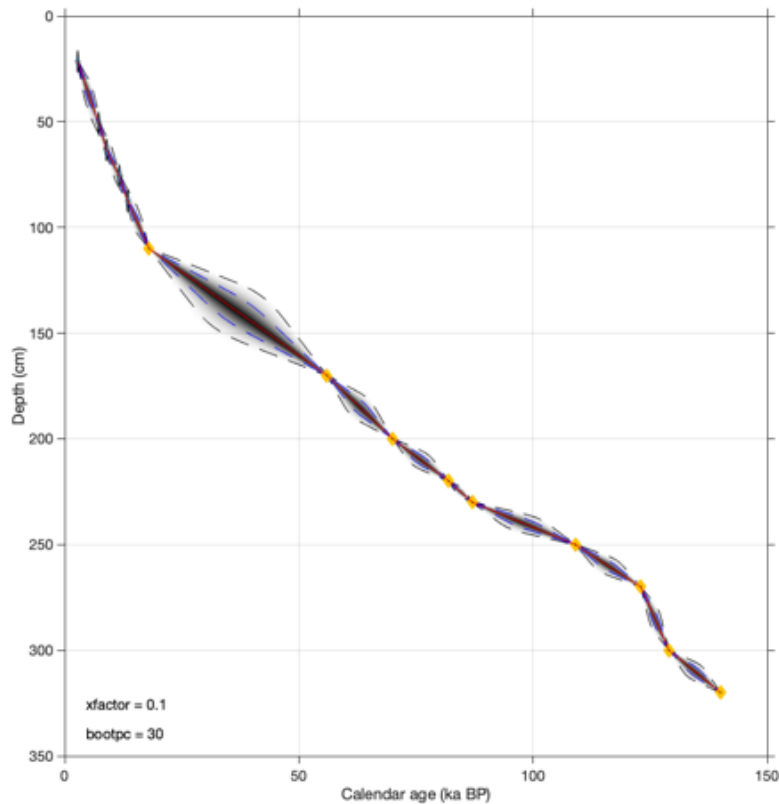
215 extends to at least 140 ka BP, capturing a full glacial-interglacial cycle. Linear sedimentation  
 216 rates (LSR) in TAN1302-96 were observed to be higher during interglacial periods, averaging  
 217  $\sim 3.5 \text{ cm ka}^{-1}$ , compared to glacial periods, averaging  $\sim 2.5 \text{ cm ka}^{-1}$ . It is worth noting that there  
 218 can be significant MRA variability over time due changes in ocean ventilation, sea ice coverage,  
 219 and wind strength, specifically in the polar high latitudes (Heaton et al., 2020), and as a result,  
 220 caution should be taken when interpreting the precision of radiocarbon dates. For more  
 221 information on age model construction and selection, refer to the supplemental online  
 222 materials (SOM).

- Deleted:
- Deleted: 3.37
- Deleted: /
- Formatted: Superscript
- Deleted: 2.74
- Deleted: /
- Formatted: Superscript



224 **Figure 2:** Age model of TAN1302-96. Red circles indicate the depth of AMS  $^{14}\text{C}$  samples and  
 225 yellow circles indicate tie points between the TAN1302-96 oxygen isotope stratigraphy and the  
 226 LR04 benthic stack (Lisiecki & Raymo, 2005). Two radiocarbon dates, OZX 519 & 520 (at 130 and  
 227 170 cm, respectively), were not included in the age model as they produced dates that were  
 228 NDFB (not distinguishable from background).

- Formatted: Not Highlight
- Deleted: <object>Figure 2:
- Deleted: stars
- Deleted: ,
- Deleted: stars
- Deleted: X
- Deleted: Y
- Deleted: ; see supplemental online materials
- Formatted: Highlight



242 **Figure 3:** Age model of TAN1302-96. Tie points are depicted as yellow dots and grey shading  
 243 represents associated uncertainty between tie points. The age model used a marine reservoir  
 244 calibration of 1000 +/- 100 years.

245

## 246 2.2 Diatom Analysis

247 TAN1302-96 was sampled every 3-4 cm throughout the core except between 130-180  
 248 cm, where samples were collected every 10 cm due to limited availability of sample materials  
 249 (Table A3 in Appendix A). Diatom slide preparation followed two procedures. The first approach

Formatted: Not Highlight

Deleted: 50

Formatted: Space Before: 6 pt, After: 6 pt, Line spacing: 1.5 lines

251 approximated the methods outlined in Renberg (1990), while the second followed the protocol  
252 outlined in Warnock & Scherer (2015). To ensure there were no biases between preparation  
253 techniques, results from each technique were first visually compared followed by a comparison  
254 of sample means (see Figure B1 in Appendix B). No biases in the data were observed between  
255 methods.

256 The first procedure was conducted at Victoria University of Wellington and Simon Fraser  
257 University on samples every 10 cm throughout the core. Sediment samples contained high  
258 concentrations of diatoms with little carbonaceous or terrigenous materials, so no dissolving  
259 aids were used. Instead, approximately 50 mg of sediment was weighed, placed into a 50 ml  
260 centrifuge tube, and topped up with 40 ml of deionized water. Samples were then manually  
261 shaken to disaggregate sediment, followed by a 10-second mechanical stir using a vortex  
262 machine. Samples were then left to settle for 25 seconds. 0.25 mL of the solution was then  
263 pipetted onto a microscope slide from a consistent depth, where it was left to dry overnight.  
264 Once the sample had dried, coverslips were permanently mounted to the slide using Permout,  
265 a high refractive index mountant. Slides were redone if they contained too many diatoms and  
266 identification was not possible, or if they contained too few diatoms (generally <40 specimens  
267 per transect). Sediment sample weight was adjusted to achieve the desired dilution.

268 The second procedure was conducted at Colgate University on samples every 3-4 cm  
269 throughout the core. Oven-dried samples were placed into a 20 ml vial with 1-2 ml of 10% H<sub>2</sub>O<sub>2</sub>  
270 and left to react for up to several days, followed by a brief (2-3 second) ultrasonic bath to  
271 disaggregate samples. The diatom solution was then added into a settling chamber, where  
272 microscope coverslips were placed on stages to collect settling diatoms. The chamber was  
273 gradually emptied through an attached spigot, and samples were evaporated overnight. Cover  
274 slips were permanently mounted onto the slides with Norland Optical Adhesive #61, a  
275 mounting medium with a high refractive index.

276 Diatom identification was conducted at Simon Fraser University using a Leica Leitz  
277 DMBRE light microscope using standard microscopy techniques. Following transverses, a  
278 minimum of 300 individual diatoms were identified at 1000x magnification from each sample  
279 throughout the core. Individuals were counted towards the total only if they represented at

Deleted: 4



281 least one-half of the specimen so that fragmented diatoms were not counted twice.  
 282 Identification was conducted to the highest taxonomic level possible, either to the species or  
 283 species-group level. Taxonomic identification was conducted using numerous identification  
 284 materials, including (but not limited to): Fenner et al. (1976); Fryxell & Hasle (1976; 1980);  
 285 Johansen & Fryxell (1985); Hasle & Syversten (1997); Cefarelli et al. (2010); and Wilks & Armand  
 286 (2017). The relative abundances were calculated by dividing the number of identified  
 287 specimens of a particular species by the total number of identified diatoms from the sample.  
 288 Based on previously established taxonomic groups (Crosta et al., 2004), diatoms were grouped  
 289 into one of three categories based on temperature preference and sea ice tolerance. The  
 290 following main taxonomic groups were used (Table 1):

- 291
- 292 [1] Sea Ice Group: representing diatoms that thrive in or near the sea ice margin in SSTs  
 293 generally ranging from -1 to 1 °C.
- 294 [2] Permanent Open Ocean Zone (POOZ): representing diatoms that thrive in open  
 295 ocean conditions, with SSTs generally ranging from ~2 to 10 °C.
- 296 [3] Sub-Antarctic Zone (SAZ): representing diatoms that thrive in warmer sub-Antarctic  
 297 waters, with SSTs generally ranging from 11 to 14 °C.

298

299 **Table 1:** Species comprising each of the diatom taxonomic groups (updated from Crosta et al.,  
 300 2004).

Sea Ice Group	POOZ Group	SAZ Group
<i>Actinocyclus actinochilus</i>	<i>Fragilariopsis kerguelensis</i>	<i>Azpeitia tabularis</i>
<i>Fragilariopsis curta</i>	<i>Fragilariopsis rhombica</i>	<i>Hemidiscus cuneiformis</i>
<i>Fragilariopsis cylindrus</i>	<i>Fragilariopsis separanda</i>	<i>Thalassionema nitzschioides</i> var. <i>lanceolata</i>
<i>Fragilariopsis obliquecostata</i>	<i>Rhizosolenia polydactyla</i> var. <i>polydactyla</i>	<i>Thalassiosira eccentrica</i>
<i>Fragilariopsis ritscheri</i>	<i>Thalassionema nitzschioides</i> (form 1)	<i>Thalassiosira oestrupii</i> gp.
<i>Fragilariopsis sublinearis</i>	<i>Thalassiosira gracilis</i> gp.	
	<i>Thalassiosira lentiginosa</i>	
	<i>Thalassiosira oliverana</i>	
	<i>Thalassiothrix</i> sp.	
	<i>Trichotoxon reinboldii</i>	

Deleted: Diatom species that have similar environmental preferences were grouped together as outlined in Crosta et al. (2004). Three main taxonomic groups were established

Deleted: , and their

Deleted: relative abundances were calculated by dividing the number of identified specimens of a particular species by the total number of identified diatoms from the sample.

Formatted: Normal

309 **2.3 Modern Analog Technique**

310 Past WSIC and SSST (January to March) were estimated for TAN1302-96 and  
311 recalculated for SO136-111 by applying the Modern Analog Technique (MAT) to the fossil  
312 diatom assemblages, as outlined in Crosta et al. (1998; 2020). Summer (January to March) SST  
313 was estimated because it is considered to be a better explanatory variable than spring or  
314 annual SST (Esper et al., 2010; Esper & Gersonde, 2014b). The MAT reference database used for  
315 this analysis is comprised of 249 modern core top samples (analogs) located primarily in the  
316 Atlantic and Indian sectors from ~40°S to the Antarctic coast. The age of the core tops included  
317 in the reference database have been assessed through radiocarbon and/or isotope stratigraphy  
318 when possible. Core tops were visually evaluated for selective diatom dissolution, so it is  
319 believed that sub-modern assemblages contain well-preserved and unbiased specimens.

320 Modern SSST and WSIC were interpolated from the reference core locations using a 1°x1° grid  
321 from the World Ocean Atlas (Locarnini et al., 2013) through the Ocean Data View (Schlitzer,  
322 2005). The MAT was applied using the “bioindic” package (Guiot & de Vernal, 2011) through the  
323 R-platform. Fossil diatom assemblages were compared to the modern analogs using 33 species  
324 or species-groups to identify the five most similar modern analogs using both the LOG and  
325 CHORD distance. The dissimilarity threshold, above which the fossil assemblages are considered  
326 to be too dissimilar to the modern dataset, is fixed at the first quartile of random distances  
327 (Crosta et al., 2020). The reconstructed SSST and WSIC are the distance-weighted mean of the  
328 climate values associated with the selected modern analog (Guiot et al., 1993; Ghadi et al.,  
329 2020). Both MAT approaches produce an R<sup>2</sup> value of 0.96 and a root mean square error of  
330 prediction (RMSEP) of ~1°C for SSST, and an R<sup>2</sup> of 0.93 and a RMSEP of 10% for WSIC (Ghadi et  
331 al. 2020). As outlined in Ferry et al., (2015), we consider <15% WSIC to represent an absence of  
332 winter sea ice, 15-40% WSIC as present but unconsolidated, and >40% to represent  
333 consolidated winter sea ice.

334 **2.4 Additional Core Data**

336 We use additional published marine cores from the southwestern Pacific throughout  
337 this analysis (Table 2), for WSIC comparisons (E27-23), %AAIW calculations (MD06-2990/SO136-

- Deleted: wSIC
- Deleted: sSST
- Deleted: s
- Deleted: s
- Deleted: were
- Deleted: they are
- Deleted: s
- Deleted: s
- Deleted: et al
- Deleted: .

- Deleted: summer
- Deleted: s
- Deleted: wSIC

- Deleted: sSST
- Deleted: wSIC

- Deleted:
- Deleted: summer
- Deleted: (mean SD = 1.28°C)
- Deleted: wSIC
- Deleted: (mean SD = 8%)
- Deleted: wSIC
- Deleted: wSIC
- Deleted:
- Formatted: Font color: Auto
- Formatted: Normal

361 [003, MD06-2986, and MD97-2120](#)), and regional SST gradient comparisons ([SO136-003](#),  
 362 [FR1/94-GC3, ODP 1119-181, DSDP 594, and Q200](#)).

363 **Table 2:** Additional data on published marine cores used throughout this analysis.

Core Name	Latitude	Longitude	Depth	Age Model Reference	Data Assessed	Data Source
<a href="#">TAN1302-96</a>	<a href="#">59.09°S</a>	<a href="#">157.05°E</a>	<a href="#">3099 m</a>	<a href="#">This study</a>	<a href="#">WSIC; SST</a>	<a href="#">This study</a>
<a href="#">SO136-111</a>	<a href="#">56.66°S</a>	<a href="#">160.23°E</a>	<a href="#">3912 m</a>	<a href="#">Crosta et al. (2004)</a>	<a href="#">WSIC; SST</a>	<a href="#">Crosta et al. (2004); recalculated in this study</a>
<a href="#">E27-23</a>	<a href="#">57.65°S</a>	<a href="#">155.23°E</a>	<a href="#">3182 m</a>	<a href="#">Ferry et al. (2015)</a>	<a href="#">WSIC</a>	<a href="#">Ferry et al. (2015)</a>
<a href="#">MD06-2990</a>	<a href="#">42.01°S</a>	<a href="#">169.92°E</a>	<a href="#">943 m</a>	<a href="#">Ronge et al. (2015)</a>	<a href="#">δ13C</a>	<a href="#">Ronge et al. (2015)</a>
<a href="#">MD06-2986</a>	<a href="#">43.45°S</a>	<a href="#">167.9°E</a>	<a href="#">1477 m</a>	<a href="#">Ronge et al. (2015)</a>	<a href="#">δ13C</a>	<a href="#">Ronge et al. (2015)</a>
<a href="#">MD97-2120</a>	<a href="#">45.54°S</a>	<a href="#">174.94°E</a>	<a href="#">121.0m</a>	<a href="#">Pahnke &amp; Zahn (2005)</a>	<a href="#">δ13C</a>	<a href="#">Pahnke &amp; Zahn (2005)</a>
<a href="#">SO136-003</a>	<a href="#">42.3°S</a>	<a href="#">169.88°E</a>	<a href="#">958 m</a>	<a href="#">Pelejero et al. (2006); Barrows et al. (2007)</a>	<a href="#">δ13C; SST</a>	<a href="#">Pelejero et al. (2006); Ronge et al. (2015)</a>
<a href="#">FR1/94-GC3</a>	<a href="#">44.25°S</a>	<a href="#">149.98°E</a>	<a href="#">2667 m</a>	<a href="#">Pelejero et al. (2006)</a>	<a href="#">SST</a>	<a href="#">Pelejero et al. (2006)</a>
<a href="#">ODP 1119-181</a>	<a href="#">44.75°S</a>	<a href="#">172.39°E</a>	<a href="#">396 m</a>	<a href="#">Wilson et al. (2005)</a>	<a href="#">SST</a>	<a href="#">Wilson et al. (2005); Hayward et al. (2008)</a>
<a href="#">DSDP 594</a>	<a href="#">45.54°S</a>	<a href="#">174.94°E</a>	<a href="#">1204 m</a>	<a href="#">Nelson et al. (1985); Kowalski &amp; Meyers (1997)</a>	<a href="#">SST</a>	<a href="#">Schaefer et al. (2005)</a>
<a href="#">Q200</a>	<a href="#">45.99°S</a>	<a href="#">172.02°E</a>	<a href="#">1370 m</a>	<a href="#">Waver et al., 1998</a>	<a href="#">SST</a>	<a href="#">Weaver et al. (1998)</a>

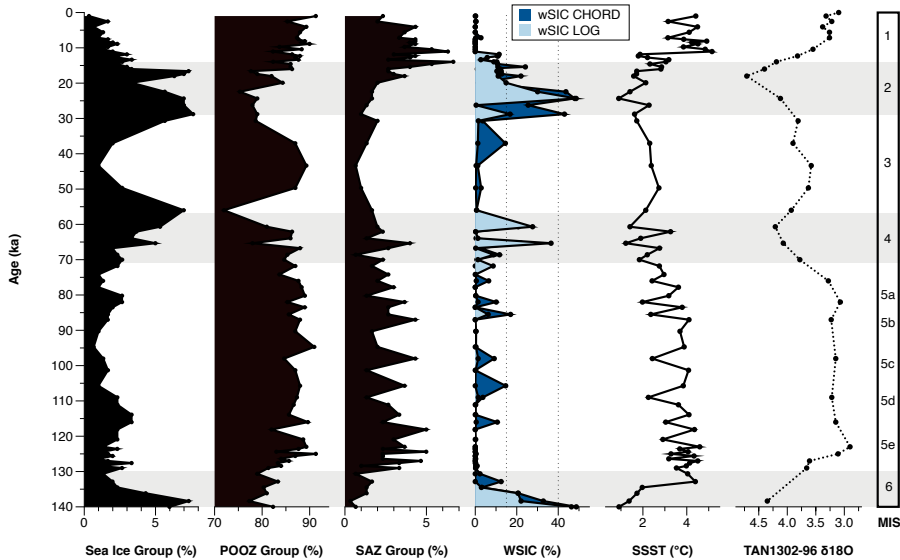
- Formatted: Font color: Auto
- Formatted: Normal, Indent: First line: 0 cm, Line spacing: single
- Formatted: Font: (Default) +Body (Calibri), 8 pt
- Formatted Table
- Formatted: Font: (Default) +Body (Calibri), 8 pt
- Formatted: Font: (Default) +Body (Calibri), 8 pt
- Formatted: Font: (Default) +Body (Calibri), 8 pt
- Formatted: Font: (Default) +Body (Calibri), 8 pt
- Formatted: Font: (Default) +Body (Calibri), 8 pt
- Formatted: Font: (Default) +Body (Calibri), 8 pt
- Formatted: Font: (Default) +Body (Calibri), 8 pt
- Formatted: Font: (Default) +Body (Calibri), 8 pt
- Formatted: Font: (Default) +Body (Calibri), 8 pt
- Formatted: Font: (Default) +Body (Calibri), 8 pt
- Formatted: Font: (Default) +Body (Calibri), 8 pt
- Formatted: Font: (Default) +Body (Calibri), 8 pt
- Formatted: Font: (Default) +Body (Calibri), 8 pt
- Formatted: Font: (Default) +Body (Calibri), 8 pt
- Formatted: Font: (Default) +Body (Calibri), 8 pt, French
- Formatted: Font: (Default) +Body (Calibri), 8 pt
- Formatted: Normal

364 **3.0 Results**

365 **3.1 [TAN1302-96](#) Diatom Assemblage Results**

366 [In this core](#), fifty-one different species or species groups were identified, of which 33  
 367 were used in the transfer function. [These 33 species represent >82% of the total diatom](#)  
 368 [assemblages \(mean of 92%\)](#). [Permanent](#) Open Ocean Zone (POOZ) diatoms made up the largest  
 369 proportion of diatoms identified, representing between 72-91% of the assemblage (Figure 4),  
 370 with higher values observed during warmer interstadial periods of MIS 1, 3, and 5. Sea ice  
 371 diatoms made up the second most abundant group, representing between 0.5-7.5% of the  
 372 assemblage, with higher values observed during cooler stadial periods (MIS 2, 4, and 6). The  
 373 Sub-Antarctic Zone group had relatively low abundances, with higher values occurring during  
 374 warmer interstadial periods ([MIS 5 and the Holocene](#)) and briefly during MIS 4 at ~65 ka BP.

- Deleted:
- Formatted: Indent: First line: 1.27 cm
- Deleted: F
- Deleted: olar
- Deleted: SAZ
- Deleted: ¶



382 **Figure 4:** Diatom assemblages results from TAN1302-96 separated into % contribution from  
 383 each taxonomic group (Sea ice Group, POOZ, and SAZ; see Table 1) over a full glacial-interglacial  
 384 cycle. Using the Modern Analog Technique (MAT), winter sea ice concentration (WSIC) and  
 385 summer sea surface temperature (SSST) were estimated and compared against the  $\delta^{18}\text{O}$   
 386 signature of TAN1302-96.

387  
 388 **3.2 TAN1302-96 SSST and WSIC Estimates**

389 There were no non-analog conditions observed in TAN1302-96 samples and all  
 390 estimates were calculated on five analogs. Estimates of SSST and WSIC from both LOG and  
 391 CHORD MAT outputs produced similar results (Figure 4). During Termination II, SSST began to  
 392 rise from ~1°C at 140 ka BP (MIS 6) to ~4.5°C at 132 ka BP (MIS 5e/6 boundary). This warming  
 393 corresponded with a decrease in WSIC from 48% to approximately 0% over the same time  
 394 periods (Figure 4). Reconstructed SSST were variable throughout MIS 5e, reaching a maximum  
 395 value of ~4.5°C at 118 ka BP, after which they declined throughout MIS 5. During this period of  
 396 SSST decline, winter sea ice was largely absent, punctuated by brief periods during which sea  
 397 ice was present but unconsolidated (WSIC = ~15% and 17% at 105 and 85 ka BP, respectively).  
 398 During MIS 4 (71 to 57 ka BP), SSST cooled to between roughly 1°C and 3°C, and sea ice

- Deleted: &
- Deleted: wSIC
- Deleted: sSST
- Deleted: ¶
- Deleted: ummer
- Deleted: wSIC
- Moved (insertion) [1]
- Deleted: sSST
- Deleted: wSIC
- Deleted: sSST
- Deleted: s
- Deleted: 0
- Deleted: wSIC
- Deleted: sSST
- Deleted: s
- Deleted: continued to rise slightly
- Deleted: 6
- Deleted: sSST
- Deleted: wSIC
- Deleted: of
- Deleted: 4.7
- Deleted: 90
- Deleted: sSST
- Deleted: s

422 expanded to 36%, such that it was present but unconsolidated for intervals of a few thousand  
423 years. SSST increased slightly from 1.5°C at 61 ka BP (during MIS 4) to ~2.5°C at 50 ka BP (during  
424 MIS 3), followed by a general cooling trend into MIS 2. Sea ice appears to have been largely  
425 absent during MIS 3 (57 to 29 ka BP), although sampling resolution is low, but increased rapidly  
426 to 48% cover during MIS 2 where winter sea ice was consolidated over the core site. During MIS  
427 2, SSST cooled to a minimum of <1°C at 24.5 ka BP. After 18 ka BP, the site rapidly transitioned  
428 from cool, ice-covered conditions to warmer, ice-free winter conditions during the early  
429 deglaciation. This warming was interrupted by a brief cooling around 13.5 ka BP, following  
430 which SSST quickly reached their maximum values of ~5°C at 11.5 ka BP and remained relatively  
431 high throughout the rest of the Holocene. Winter sea ice was not present during the Holocene.

### 3.3 SO136-111 SSST and WSIC Recalculation

434 In core SO136-111, the 33 species included in the transfer function represent values  
435 >79% of the total diatom assemblages (mean of 91%). There were no non-analog conditions  
436 observed in SO136-111 samples and all estimates were calculated on five analogs. Recalculated  
437 estimates of SSST and WSIC from both LOG and CHORD MAT outputs produced similar results  
438 for SO136-111 (Figure 5a, 5d). During Termination II, SSST rose from ~2°C at 137 ka BP (MIS 6)  
439 to a maximum value of 6°C at 125 ka BP (MIS 5e), corresponding to a rapid decline in WSIC from  
440 37% to ~0% during the same period. SSST remained relatively high (between 4 and 5°C) from  
441 125 ka BP until 115 ka BP where they declined to ~2°C. SSST remained variable from 110 ka BP  
442 until ~40 ka BP, fluctuating between ~2°C and 4°C. Winter sea ice was largely absent during MIS  
443 5, with a brief period where sea ice was present but unconsolidated (WSIC = 17% at 84 ka).  
444 Beginning at ~76 ka BP, WSIC began to increase and continued throughout early MIS 4 to a  
445 maximum 36% at 69 ka BP. WSIC remained present but unconsolidated throughout most of MIS  
446 3 and 2 with brief periods of absence (WSIC = <15%) lasting a few thousand years. SSST and  
447 WSIC reached their coolest values and highest concentration at 24.5 ka before SSST increased  
448 to ~5°C and stabilized throughout the Holocene, while WSIC declined to virtually 0% throughout  
449 the same period. ↓

Deleted: SSST

Deleted: s

Deleted: sSSST

Deleted: s

Deleted: sSSST

Deleted: s

Deleted: 4

Moved up [1]: There were no non-analog conditions observed in TAN1302-96 samples.

Formatted: Normal

Deleted: Similar to TAN1302-96, r

Deleted:

Deleted: s

Deleted: s

Deleted: s

Deleted: s

Deleted: s

Deleted: s

Deleted: There were no non-analog conditions observed in SO136-111 samples.

Formatted: Normal, Space Before: 6 pt, After: 6 pt, Line spacing: 1.5 lines

470 **4.0 Discussion**

471 **4.1 Regional sSST and WSIC Estimates**

472 The new WSIC and sSST estimates from TAN1302-96 and recalculated WSIC estimates  
473 from SO136-111 show a coherent regional pattern (Figure 5). TAN1302-96 shows slightly higher  
474 concentrations during MIS 2 (max WSIC = 43% at 24.5 ka BP) and 4 (max WSIC = 37% at 65 ka  
475 BP) compared with SO136-111 (max WSIC = 35% at 24.5 ka BP and 36% at 68 ka BP,  
476 respectively), which can be explained by a more poleward position of TAN1302-96 relative to  
477 SO136-111. The estimates between cores differ during MIS 3, with seemingly lower WSIC in  
478 TAN1302-96 than in SO136-111, which might result from the low sampling resolution in  
479 TAN1302-96 during this period. Overall, these cores show a highly similar and coherent history  
480 of sea ice over the last 140 ka BP.

Deleted: sSST

Deleted: wSIC

Deleted: wSIC

Deleted: sSST

Deleted: wSIC

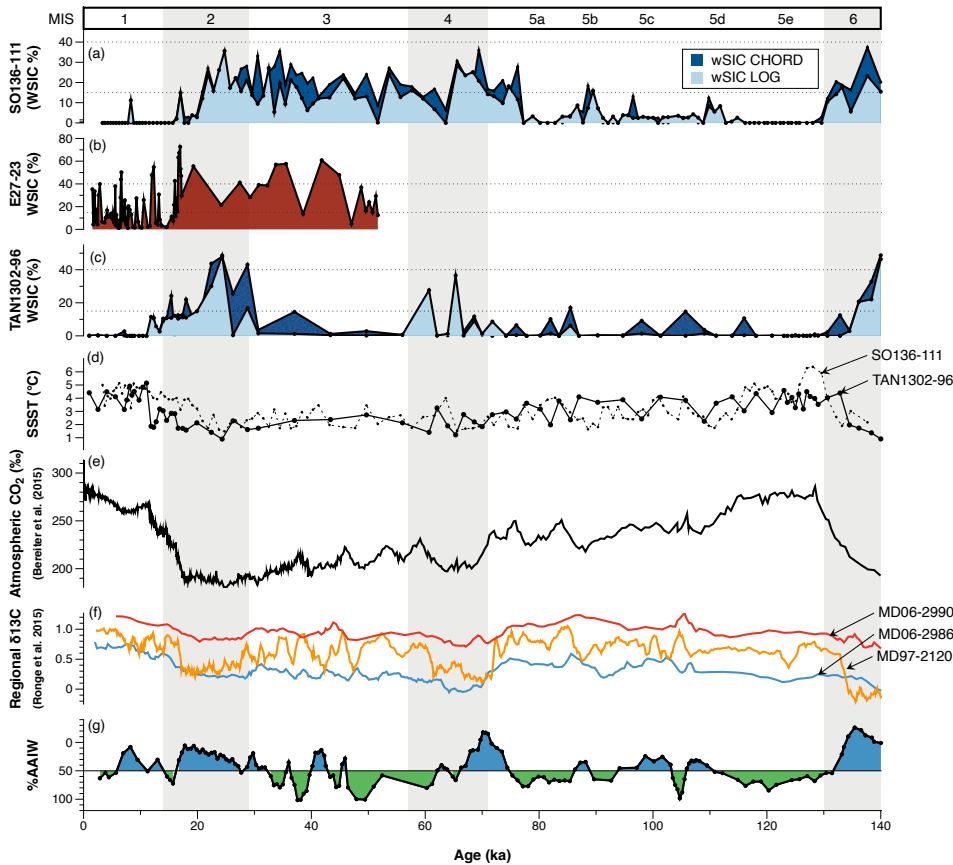
Deleted: Both cores show relatively high concentrations of sea ice during MIS 2, 4, and 6, with lower values during MIS 1 and 5. ...

Deleted: 7

Deleted: wSIC

Deleted: ¶

Formatted: Indent: First line: 1.27 cm, Line spacing: 1.5 lines



493 **Figure 5:** (a) wSIC estimates using MAT from SO136-111 (recalculated in this study, see  
 494 Appendix D); (b) wSIC estimates using GAM from E27-23 (Ferry et al., 2015); (c) wSIC estimates  
 495 using MAT from TAN1302-96 (this study); (d) SSST estimates using MAT from TAN1302-96 (solid  
 496 black line) and recalculated SSST for SO136-111 (black dotted line); (e) Antarctic atmospheric  
 497 CO<sub>2</sub> concentrations over 140 ka BP (Bereiter et al., 2015); (f) δ<sup>13</sup>C data from nearby cores  
 498 MD06-2990/SO136-003, MD97-2120, and MD06-2986 (Ronge et al., 2015); (g) %Antarctic  
 499 Intermediate Water (%AAIW) as calculated in Ronge et al. (2015), which tracks when core  
 500 MD97-2120 was bathed primarily by AAIW (green) or Upper Circumpolar Deep Water (UCDW)  
 501 (blue).  
 502

- Deleted: wSIC
- Deleted: wSIC
- Deleted: wSIC
- Deleted: sSST
- Deleted: this study

508 When compared with E27-23 (Figure 5b), which is located only ~120 km to the  
 509 southwest of TAN1302-96 (Figure 1), the TAN1302-96 core shows lower estimates of ~~WSIC~~,  
 510 especially during MIS 3. During early and mid-MIS 2, both cores show similar ~~WSIC~~ estimates,  
 511 while later in MIS 2 (~17 ka ~~BP~~), E27-23 reports a maximum ~~WSIC~~ of 72% compared to only 22%  
 512 at TAN1302-96. A discrepancy between estimates is also observed during the Holocene, with  
 513 E27-23 reporting sea ice estimates of up to nearly 50% during the mid-Holocene (~6 ka ~~BP~~),  
 514 while TAN1302-96 experienced values well below the RMSEP of 10%.

515 Possible explanations for the observed differences in ~~WSIC~~ estimates include: [1]  
 516 ~~differences in statistical applications~~; [2] ~~lateral sediment redistribution~~; [3] ~~differences in~~  
 517 ~~laboratory protocols~~; [4] ~~differences in diatom identification/counting methodology~~; and [5]  
 518 ~~selective diatom dissolution~~. Of these explanations, we believe that [1] and [2] are the most  
 519 likely candidates and are discussed below (for further discussion on [3], [4], and [5], see  
 520 Appendix C).

521 The first possible explanation is the use of different statistical applications. Ferry et al.  
 522 (2015) used a Generalized Additive Model (GAM) to estimate ~~WSIC~~ for both E27-23 and SO136-  
 523 111, while we have used the MAT for TAN1302-96 and SO136-111. A simple comparison of  
 524 ~~WSIC~~ estimates between the results in Ferry et al. (2015) and our recalculated ~~WSIC~~ estimates  
 525 for SO136-111 can provide insights into the magnitude of estimation differences. Generally  
 526 speaking, the GAM estimation produced higher ~~WSIC~~ estimates than the MAT (e.g., ~50% ~~WSIC~~  
 527 at 23 ka ~~BP~~ while the MAT produced ~37% for the same time period); however, we believe it is  
 528 unlikely that statistical approaches alone could explain a larger difference (i.e., 50%) between  
 529 E27-23 and TAN1302-96.

530 The second possible explanation involves lateral sediment redistribution and focusing by  
 531 the ACC. We estimated sediment focusing for E27-23 using <sup>230</sup>Th data from Bradtmiller et al.  
 532 (2009) together with dry bulk density estimated using calcium carbonate content (Froelich,  
 533 1991). Both sedimentation rates and focusing factors (~~FF~~) for the E27-23 are relatively high  
 534 (~~max.~~ = ~35 cm ~~ka~~<sup>-1</sup> and 26, respectively) during the LGM and Holocene, which could influence  
 535 the reliability of ~~WSIC~~ and ~~SSST~~ estimation (see Figure B2 in Appendix B). Several peaks in  
 536 focusing occurring around 16, 12, and 3 ka ~~BP~~ appear to closely correspond to periods of peak

Deleted: wSIC

Deleted: wSIC

Deleted: wSIC

Deleted: wSIC

Deleted: differences in laboratory protocols

Deleted: differences in diatom identification/counting methodology;...

Deleted: differences in statistical applications

Deleted: selective diatom dissolution

Deleted: differences in the redistribution of sediment by the Antarctic Circumpolar Current (ACC) between each of the core sites...

Deleted: 3

Deleted: 5

Deleted: 1

Deleted: [

Deleted: 2

Deleted: 4

Deleted: we identified

Deleted: through

Deleted: wSIC

Deleted: wSIC

Deleted: wSIC

Deleted: wSIC

Deleted: wSIC

Deleted: is through

Deleted: /

Formatted: Superscript

Deleted: max=

Deleted: wSIC

Deleted: sSST



567 wSIC (~67%, ~54%, and ~35%, respectively), suggesting a possible link. Lateral redistribution  
568 could artificially increase or decrease relative abundances of some diatom groups, which could  
569 lead to over- or under-estimations of sea ice coverage. Thorium analysis for TAN1302-96 is  
570 beyond the scope of this study; however, future work could help address this uncertainty.

Deleted: wSIC

Deleted: under

571 Although we are unable to identify the specific cause of the differences, we suggest  
572 considering the results from all cores when drawing conclusions of regional sea ice history.

Deleted: do

Deleted: using caution when interpreting the exact magnitude of sea ice expansion in this region, and

Deleted: to

Formatted: Normal

## 574 4.2 The Role of Sea Ice on Early CO<sub>2</sub> Drawdown

575 Kohfeld & Chase (2017) hypothesized that the initial drawdown of atmospheric CO<sub>2</sub> (~35  
576 ppm) during the glacial inception of MIS 5d (~115 to 100 ka BP) was primarily driven by sea ice  
577 capping and a corresponding stratification of surface waters, which reduced the CO<sub>2</sub> outgassing  
578 of upwelled carbon-rich waters. This hypothesis is supported by several lines of evidence,  
579 including: [1] sea salt sodium (ssNA) archived in Antarctic ice cores, suggesting sea ice  
580 expansion near the Antarctic continent (Wolf et al., 2010); [2]  $\delta^{15}\text{N}$  proxy data from the central  
581 Pacific sector of the Southern Ocean, suggesting increased stratification south of the modern-  
582 day Antarctic Polar Front (Studer et al., 2015); and [3] diatom assemblages in the Permanent  
583 Open Ocean Zone (POOZ) of the Atlantic sector, suggesting a slight cooling and northward  
584 expansion of sea ice during MIS 5d (Bianchi & Gersonde, 2002). Our data address this  
585 hypothesis by providing insights into early sea ice expansion into the polar frontal zone of the  
586 western Pacific sector.

Deleted: polar frontal

Deleted: z

Deleted: ,

587 Our data show that, in contrast to the Atlantic sector (Bianchi & Gersonde, 2002), there  
588 does not appear to be any evidence of sea ice expansion in the southwestern Pacific during MIS  
589 5d at either the TAN1302-96 or SO136-111 core sites (Figure 5). Unfortunately, the lack of  
590 spatially extensive quantitative records extending back to Termination II limits our ability to  
591 estimate the timing and magnitude of sea ice changes for regions poleward of 59°S in the  
592 southwestern Pacific. We anticipate, however, that an advance in the sea ice edge, consistent  
593 with those outlined in Bianchi and Gersonde (2002), likely would have reduced local SST, as the  
594 sea ice edge advanced closer to the core site. Indeed, the TAN1302-96 SST record does show a  
595 decrease to ~2°C (observed at 108 ka BP), which quickly rebounded to ~4°C by ~102 ka BP.

Deleted: →

Deleted: was no

Deleted: ice advance

Deleted: into the modern-day PFZ of the

Deleted: SW

Deleted: . Neither

Deleted: nor

Deleted: 0

Deleted: shows evidence of an early glacial increase in wSIC

Deleted: &

Deleted: s

Deleted: 7

Deleted: 5

618 (Figure 5). However, this ~~SSST~~ drop occurred roughly 7 ka BP after the initial CO<sub>2</sub> reduction,  
619 suggesting that the CO<sub>2</sub> drawdown event and local ~~SSST~~ reduction may not be linked. ~~Thus,~~  
620 ~~while we cannot rule out the possibility of modest sea ice advances or consolidation of pre-~~  
621 ~~existing sea ice (particularly to the south of the core sites), the quantitative WSI and SSST~~  
622 ~~reconstructions suggest that sea ice cover over our core site was limited during glacial~~  
623 ~~inception.~~

624 Given that sea ice was not at its maximum extent during the early glacial, it stands to  
625 reason that any reductions to air-sea gas exchange in response to the hypothetically expanded  
626 sea ice would not have been at its maximum impact either. ~~Previous modeling work has~~  
627 ~~suggested that the maximum impact of sea ice expansion on glacial-interglacial atmospheric~~  
628 ~~CO<sub>2</sub> reductions ranged from 5 to 14 ppm (Kohfeld and Ridgwell, 2009). More recent modeling~~  
629 ~~studies are consistent with this range, suggesting a 10 ppm reduction (Stein et al., 2020), while~~  
630 ~~some studies even suggest a possible increase in atmospheric CO<sub>2</sub> concentrations due to sea ice~~  
631 ~~expansion (Khatiwala et al., 2019). Furthermore, Stein et al. (2020) suggest that the effects of~~  
632 ~~sea ice capping would have taken place after changes in deep ocean stratification had occurred~~  
633 ~~and would have contributed to CO<sub>2</sub> drawdown later during the mid-glacial period. These model~~  
634 ~~results, when combined with our data, suggest that even if modest sea ice advances did take~~  
635 ~~place during the early glacial (i.e., MIS 5d), their impacts on CO<sub>2</sub> variability likely would have~~  
636 ~~been modest, ultimately casting doubt on the hypothesis that early glacial CO<sub>2</sub> reductions of 35~~  
637 ~~ppm can be linked solely to the capping and stratification effects of sea ice expansion.~~

### 638 **4.3 Other Potential Contributors to Early Glacial CO<sub>2</sub> Variability**

640 The changes observed in ~~WSIC~~ and ~~SSST~~ from TAN1302-96 suggest that sea ice  
641 expansion was likely not extensive enough early in the glacial cycle for a sea ice capping effect  
642 to be solely responsible for early atmospheric CO<sub>2</sub> drawdown. This leaves open the question of  
643 what may have contributed to early drawdown of atmospheric CO<sub>2</sub>. In terms of the ocean's  
644 role, we highlight three contenders: [1] a potentially non-linear response between sea ice  
645 coverage and CO<sub>2</sub> sequestration potential; [2] links between sea ice expansion and early

Deleted: sSST

Deleted: 8

Deleted: sSST

Deleted: While the lack of sea ice diatoms and no discernable reductions of sSSTs occurred during MIS 5d at TAN1302-96 or SO136-111, we cannot rule out the possibility that modest sea ice advances, or a consolidation of pre-existing sea ice, took place south of the core sites.

Formatted: Font: (Default) +Body (Calibri)

Deleted: Thus, it is likely that any effects of sea ice capping would not have reached their full potential during the early glacial period. ...

Deleted: &

Deleted: -

Deleted: likely

Formatted: Normal

Deleted: wSIC

Deleted: sSST

Deleted: s

663 changes in global ocean overturning, and [3] the impact of cooling on air-sea disequilibrium in  
664 the Southern Ocean.

665 The first possible explanation considers that not all sea ice has the same capacity to  
666 facilitate or inhibit air-sea gas exchange. We previously suggested that because sea ice was not  
667 at its maximum extent during MIS 5d, the contribution of sea ice on CO<sub>2</sub> sequestration would  
668 likely not be at its maximum extent either. However, this assumes a linear relationship between  
669 sea ice coverage and CO<sub>2</sub> sequestration potential. We know that different sea ice properties,  
670 such as thickness and temperature, determine overall porosity, with thicker and colder sea ice  
671 being less porous and more effective at reducing air-sea gas exchange compared to thinner and  
672 warmer sea ice (Delille et al., 2014). It is therefore possible that if modest sea ice advances took  
673 place closer to the Antarctic continent (and were therefore not captured by TAN1302-96), they  
674 may have been more effective at reducing CO<sub>2</sub> outgassing, either by experiencing some type of  
675 reorganization or consolidation, or through a change in properties such as temperature or  
676 thickness. It is also possible that sea ice coverage over some regions leads to more effective  
677 capping, while in other regions sea ice growth contributes only to marginal reductions in air-sea  
678 gas exchange. This, theoretically, could point to a non-linear response between sea ice  
679 expansion and CO<sub>2</sub> sequestration potential, and thus modest sea ice growth around the  
680 Antarctic continent could have contributed in part to the ~35 ppm initial CO<sub>2</sub> drawdown event.  
681 While this is theoretical and cannot be adequately addressed in this analysis, it is worthy of  
682 deeper consideration.

683 The second possible explanation involves changes in the global overturning circulation.  
684 Kohfeld and Chase (2017) previously examined the timing of changes in δ<sup>13</sup>C of benthic  
685 foraminifera solely from the Atlantic basin and observed that the largest changes in the Atlantic  
686 Meridional Overturning Circulation (AMOC) coincided with the mid-glacial reductions in  
687 atmospheric CO<sub>2</sub> changes mentioned above. Subsequent work of O'Neill et al. (2020) examined  
688 whole-ocean changes in δ<sup>13</sup>C of benthic foraminifera and noted that the separation between  
689 δ<sup>13</sup>C values of abyssal and deep ocean waters - and therefore the isolation of the abyssal ocean  
690 - was actually initiated between MIS 5d and MIS 5a (114 to 71 ka BP). Evidence for early  
691 changes in abyssal circulation and reductions in deep-ocean overturning have also been

Deleted: that there is

Deleted: ,

Deleted: could link

Deleted: &

Deleted: carbon dioxide

Formatted: Subscript

Deleted: were

698 detected in Indian Ocean  $\delta^{13}\text{C}$  records (Govin et al., 2009). More recently, Indian Ocean  $\epsilon\text{Nd}$   
699 records (Williams et al., 2021) have suggested that the abyssal ocean may have responded to  
700 sea ice changes around the Antarctic continent early in the glacial cycle, with colder and more  
701 saline AABW forming as sea ice expanded near the continent. If indications of an early-glacial  
702 response in the global ocean circulation in the Indo-Pacific are correct, these data may also  
703 point to an elevated importance of sea ice near the Antarctic continent in triggering early,  
704 deep-ocean overturning changes.

705 The third possible explanation involves changes in surface ocean temperature gradients  
706 in the Southern Ocean, and how they could influence air-sea gas exchange. Several recent  
707 studies have pointed to the importance of changes to air-sea disequilibrium as a key  
708 contributor to  $\text{CO}_2$  uptake in the Southern Ocean (Eggleston & Galbraith, 2018; Marzocchi &  
709 Jansen 2019; Khatiwala et al. 2019). Khatiwala et al. (2019) suggested that modelling studies  
710 have traditionally underrepresented (or neglected) the role of air-sea disequilibrium in  
711 amplifying the impact of cooling on potential  $\text{CO}_2$  sequestration in the mid-high southern  
712 latitudes during glacial periods. They argue that when the full effects of air-sea disequilibrium  
713 are considered, ocean cooling can result in a 44 ppm decrease due to temperature-based  
714 solubility effects alone. They attributed this increased impact of SST to a reduction in sea-  
715 surface temperature gradients explicitly in polar mid-latitude regions (roughly between  $40^\circ$  and  
716  $60^\circ$  north and south). If we compare the SST gradients in the southwest Pacific sector over the  
717 last glacial-interglacial cycle (Figure 6), we see an early cooling response between MIS 5e-d  
718 corresponding to roughly half of the full glacial cooling, specifically in the cores located south of  
719 the modern STF. While not quantified, Bianchi and Gersonde (2002) also described a weakening  
720 of meridional SST gradients between the Subantarctic and Antarctic Zones during MIS 5d in the  
721 Atlantic sector. Although this analysis is based on sparse data, our SSST reconstructions are  
722 consistent with the notion that surface ocean cooling, a weakening of meridional SST gradients,  
723 and changes to the overall air-sea disequilibrium could be responsible for at least some portion  
724 of the early  $\text{CO}_2$  drawdown. Further SST estimates from the region, and from the global ocean,  
725 are needed to substantiate this hypothesis.

Deleted: , and

Deleted: m

Deleted: in

Deleted: , suggesting

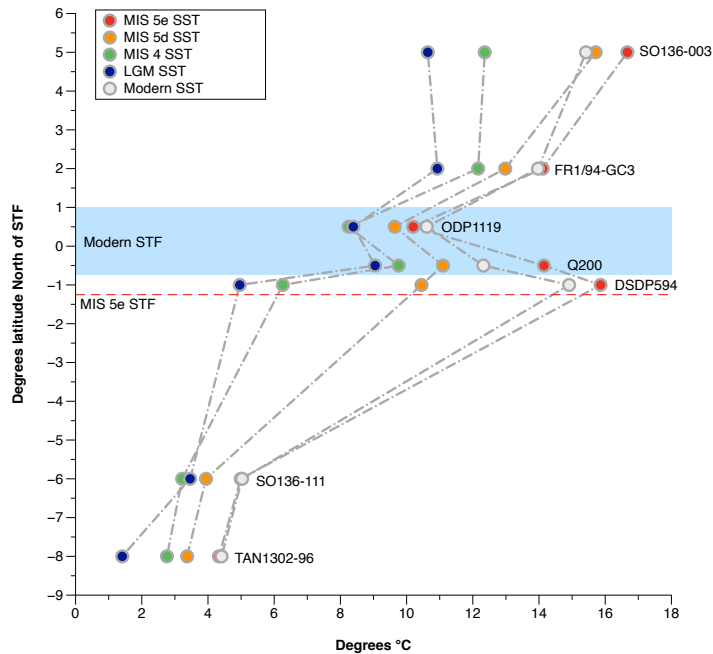
Deleted: .

Deleted: s

Deleted: (for core list, see Table B1 in Appendix B)

Deleted: &

Deleted: idea



735 **Figure 6:** SST estimates from 7 cores located in the southwestern Pacific. SST<sub>u</sub> used were 5-point  
 736 averages (depending on sampling resolution) taken at MIS peaks/median dates in accordance  
 737 with boundaries outlined in Lisiecki & Raymo, (2005). Due to the complex circulation and  
 738 frontal structures in the region, cores were plotted in +/- distance from the average position of  
 739 the modern STF. Cores used include: SO136-003 (SSTs calculated from alkenones, Pelejero et  
 740 al., 2006); FR1/94-GC3 (alkenones, Pelejero et al., 2006); ODP 181-1119 (PF-MAT, Hayward et  
 741 al., 2008); DSDP594 (PF-MAT, Schaefer et al., 2005); Q200 (PF-MAT, Weaver et al., 1998);  
 742 SO136-111 (D-MAT, Crosta et al., 2004); and TAN1302-96 (D-MAT; *this study*). The blue band  
 743 represents the modern STF zone while the red dotted line represents the southern shift in the  
 744 STF during MIS 5e (Cortese et al., 2013).

Deleted: s

Deleted: GC3

Formatted: Normal

#### 746 4.4 Sea Ice Expansion and Ocean Circulation

747 Although the TAN1302-96 WSIC record suggests that sea ice was largely absent at the  
 748 core site until the mid-glacial (~65 ka BP), the observed changes in sea ice could have  
 749 modulated regional fluctuations in Antarctic Intermediate Water (AAIW) subduction  
 750 throughout the glacial-interglacial cycle. The annual growth and decay of Antarctic sea ice plays

Deleted: wSIC

Deleted: throughout the glacial-interglacial cycle

Deleted: may be linked to

756 a critical role in regional water mass formation. Brine rejection results in net buoyancy loss in  
757 regions of sea ice formation, while subsequent melt results in freshwater inputs and net  
758 buoyancy gains near the ice margin (Shin et al., 2003; Pellichero et al., 2018). This increased  
759 freshwater input and buoyancy gain near the ice margin can hinder AAIW subduction, with  
760 direct and indirect impacts on both the upper and lower branches of the meridional  
761 overturning circulation (Pellichero et al. 2018).

762 Previous research has used  $\delta^{13}\text{C}$  in benthic foraminifera to track changes in the depth of  
763 the interface between AAIW and Upper Circumpolar Deep Water (UCDW) (Pahnke and Zahn,  
764 2005; Ronge et al., 2015). Low  $\delta^{13}\text{C}$  values are linked to high\_nutrient concentrations found at  
765 depths below ~1500 m in the UCDW, and higher  $\delta^{13}\text{C}$  values are associated with the shallower  
766 AAIW waters (Figure 5). Marine sediment core MD97-2120 (45.535°S, 174.9403°E, core depth  
767 1210 m) was retrieved from a water depth near the interface between the AAIW and UCDW  
768 water masses (Pahnke & Zahn, 2005). Over the last glacial-interglacial cycle, fluctuations in the  
769 benthic  $\delta^{13}\text{C}$  values from MD97-2120 suggest that the core site was intermittently bathed in  
770 AAIW and UCDW, and that the vertical extent of AAIW fluctuated throughout the last glacial-  
771 interglacial cycle. Ronge et al. (2015) used the  $\delta^{13}\text{C}$  values from MD97-2120 and other core sites  
772 to quantify the contributions of AAIW to the waters overlying MD97-2120 (%AAIW, Appendix  
773 D). These results suggest that during warm periods, MD97- 2120 exhibited more positive  $\delta^{13}\text{C}$   
774 values, corresponding to higher %AAIW, while cooler periods exhibited more negative values,  
775 corresponding to lower %AAIW (Figure 5). This suggests that during cooler periods, the AAIW-  
776 UCDW interface shoaled, reducing the total volume of AAIW and indirectly causing an  
777 expansion of UCDW (Ronge et al., 2015).

778 Our comparison between %AAIW and regional WSIC estimates suggest a strong link  
779 between the two (Figure 5). Specifically, we observe that AAIW shoaled and UCDW expanded  
780 (i.e., %AAIW is low) during periods when sea ice expansion occurred. In contrast, during periods  
781 of low WSIC, a reduced seasonal sea ice cycle, and warmer summer sea surface temperatures  
782 (e.g., MIS 5e), %AAIW is observed to be high. This correlation supports the idea that increased  
783 concentrations of regional sea ice resulted in a substantial summer freshwater flux into the  
784 AAIW source region. This regional freshening likely promoted a shallower subduction of AAIW

Deleted: s

Deleted: means

Deleted: wSIC

Deleted: sea ice expansion occurs during time periods when

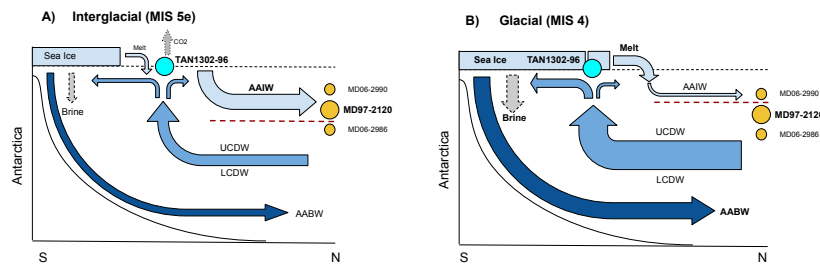
Deleted: has

Deleted: has

Deleted: time

Deleted: wSIC

793 and a corresponding volumetric expansion of UCDW, which can be seen by the isotopic offset  
 794 of the  $\delta^{13}\text{C}$  values between the reference cores, and also by the increased carbonate dissolution  
 795 in MD97-2120 during glacial periods (Figure 7) (Pahnke et al., 2003; Ronge et al., 2015). These  
 796 findings directly link sea ice proxy records to observed changes in ocean circulation and water  
 797 mass geometry.



799  
 800 **Figure 7:** Schematic of changes in southwestern Pacific sector sea ice coverage and water mass  
 801 geometry between interglacial and glacial stages. **A)** Depicts interglacial conditions where sea  
 802 ice coverage is minimal and freshwater input from summer sea ice melt is low. This lack of  
 803 freshwater input allows AAIW to subduct to deeper depths and bath core MD97-2120,  
 804 capturing the higher  $\delta^{13}\text{C}$  signature of the overlying AAIW waters. The AAIW-UCDW interface  
 805 (red dashed line) is located beneath MD97-2120.  $\text{CO}_2$  outgassing is occurring as carbon-rich  
 806 Circumpolar Deep Waters upwell near Antarctica. **B)** Depicts glacial conditions where sea ice  
 807 expansion has occurred beyond TAN1302-96, increasing brine rejection, and stabilizing the  
 808 water column. As a result of the increased sea ice growth, subsequent summer melt increases  
 809 the freshwater flux into the AAIW source region and increases AAIW buoyancy. This buoyancy  
 810 gain shoals the AAIW-UCDW interface above core MD97-2120, causing the core site to be  
 811 bathed in low  $\delta^{13}\text{C}$  UCDW. The shoaling of AAIW causes an indirect expansion of CDW,  
 812 increasing the glacial carbon stocks of the deep ocean while sea ice reduces  $\text{CO}_2$  outgassing via  
 813 the capping mechanism.

814  
 815 In addition to its influence on regional freshwater forcing and AAIW reductions, these  
 816 sea ice changes may also coincide with larger-scale deep ocean circulation changes. The most  
 817 dramatic increases in winter sea ice observed in TAN1302-96 and SO136-111, along with  
 818 changes in %AAIW, are initiated during MIS 4. These shifts also correspond to basin-wide

Formatted: Indent: First line: 0 cm

819 changes in benthic  $\delta^{13}\text{C}$  values in the Atlantic Ocean that suggest a shoaling in the AMOC during  
820 MIS 4 (Oliver et al., 2010; Kohfeld & Chase, 2017). Changes in deep ocean circulation are also  
821 recorded in  $\epsilon\text{Nd}$  isotope data in the Indian sector of the Southern Ocean (Wilson et al., 2015),  
822 suggesting extensive reductions in the AMOC during this period. Recent modelling literature  
823 (Marzocchi & Jansen, 2019; Stein et al., 2020) suggests that sea ice formation directly impacts  
824 marine carbon storage by increasing density stratification and reducing diapycnal mixing,  
825 especially in simulations where brine rejection is enhanced near the Antarctic continental slope  
826 and open ocean vertical mixing (and subsequent  $\text{CO}_2$  outgassing) is reduced (Bouttes et al.  
827 2010; 2012; Menviel et al. 2012). These simulations suggest a resulting  $\text{CO}_2$  sequestration of  
828 20-40 ppm into the deep ocean.

829 Taken collectively, the available data show that sea ice expansion, AAIW-UCDW  
830 shoaling, changes in the AMOC, and a decrease in atmospheric  $\text{CO}_2$  all occur concomitantly  
831 during MIS 4 (Figure 5). It appears likely, therefore, that sea ice expansion during this time  
832 influenced intermediate water density gradients through increased freshening and consequent  
833 shoaling of AAIW, which may also have increased the efficiency of the carbon pump and  
834 increased  $\text{CO}_2$  uptake by phytoplankton (Sigman et al., 2021). This appears to have occurred  
835 while simultaneously influencing deep-ocean density, and therefore stratification, through  
836 brine rejection and enhanced deep water formation, which ultimately lead to decreased  
837 ventilation (Abernathey et al., 2016). These changes in ocean stratification, combined with the  
838 sea ice 'capping' mechanism, appear to agree with both the recent modelling efforts (Stein et  
839 al., 2020) and observed proxy data, and fit well within the hypothesis that mid-glacial  $\text{CO}_2$   
840 variability was primarily the result of a more sluggish overturning circulation (Kohfeld & Chase,  
841 2017).

## 842 5.0 Summary & Conclusion

844 This study presents new WSIC and SSST estimates from marine core TAN1302-96,  
845 located in the southwestern Pacific sector of the Southern Ocean. We find that the WSIC  
846 remained low during the early glacial cycle (130 to 70 ka BP), expanded during the middle  
847 glacial cycle (~65 ka BP), and reached its maximum just prior to the LGM (~24.5 ka BP). These

Deleted: Atlantic Meridional Overturning Circulation (  
Deleted: )

Deleted: changes

Deleted: ?

Formatted: Subscript

Deleted: (Menviel et al., 2012)

Deleted: , ultimately leading to

Deleted: an estimated 30

Deleted: {Bouttes, 2010 #5595}

Formatted: Subscript

Deleted: wSIC

Deleted: sSST

Deleted: wSIC



859 results largely agree with nearby core SO136-111 but display some differences in WSIC  
860 magnitude with E27-23. This discrepancy may be explained by differences in statistical  
861 applications and/or lateral sediment redistribution, although more analysis is required to  
862 determine the exact cause(s).

Deleted: wSIC

863 The lack of changes in sSST and the absence of winter sea ice over the core site during  
864 the early glacial suggests that the sea ice capping mechanism and corresponding surface  
865 stratification in this region is an unlikely cause for early CO<sub>2</sub> drawdown, and that alternative  
866 hypotheses should be considered when evaluating the mechanism(s) responsible for the initial  
867 drawdown. More specifically, we consider the impact of changes in sSST gradients between  
868 ~40° to 60°S and support the idea that changes in air-sea disequilibrium associated with  
869 reduced sea-surface temperature gradients could be a potential mechanism that contributed to  
870 early glacial reductions in atmospheric CO<sub>2</sub> concentrations (Khatiwala et al., 2019). Another key  
871 consideration is the potentially non-linear response between sea ice expansion and CO<sub>2</sub>  
872 sequestration potential (i.e., that not all sea ice is equal in its capacity to sequester carbon).  
873 More analyses are required to adequately address this.

Deleted: sSST

Deleted: s

874 We also observe a strong link between regional sea ice concentrations and vertical  
875 fluctuations in the AAIW-UCDW interface. Regional sea ice expansion appears to coincide with  
876 the shoaling of AAIW, likely due to the freshwater flux from summer sea ice melt increasing  
877 buoyancy in the AAIW formation region. Furthermore, major sea ice expansion and AAIW  
878 shoaling occurs during the middle of the glacial cycle and is coincident with previously  
879 recognized shoaling in AMOC and mid-glacial atmospheric CO<sub>2</sub> reductions, suggesting a  
880 mechanistic link between sea ice and ocean circulation.

881 In conclusion, this paper has focused exclusively on sea ice as a driver of physical  
882 changes, but we recognize that these changes in sea ice will be accompanied by multiple  
883 processes that interact and compete with each other. Marzocchi & Jansen (2019) note that  
884 teasing apart the individual components of CO<sub>2</sub> fluctuations is complicated because of  
885 interactions between sea ice capping, air-sea disequilibrium, AABW formation rates, and the  
886 biological pump. We recognize that these processes may not act independently, and as such,

Deleted: T

891 have contributed new data to help advance our collective understanding of the role of sea ice  
 892 on influencing atmospheric CO<sub>2</sub> variability on a glacial-interglacial time scale.

Deleted: hope to

893

Formatted: Normal

## 894 6.0 Appendices

### 895 Appendix A: Age Model & Sampling Depths

896 **Table A1:** Radiocarbon dates taken from TAN1302-96. NDFB = Not Distinguishable from Background

Deleted: -

Lab Code	Sample Material	Core Name	Depth (cm)	δ13C (per mil)	δ13C (+/-)	% Modern Carbon	1σ error	Fraction Modern	(+/-)	Radiocarbon Year	1σ error	Reference
NZA 57105	<i>N. pachyderma</i> and <i>G. bulloides</i>	TAN1302-96	21	1	0.2	/	/	0.5982	0.0018	4127	24	Prebble et al., 2017
NZA 57109	<i>N. pachyderma</i> and <i>G. bulloides</i>	TAN1302-96	50	0.7	0.2	/	/	0.3723	0.0015	7936	32	Prebble et al., 2017
OZX 517	<i>N. pachyderma</i> and <i>G. bulloides</i>	TAN1302-96	63	1	0.1	30.62	0.15	/	/	9505	40	This study
NZA 61429	<i>N. pachyderma</i> and <i>G. bulloides</i>	TAN1302-96	75	0.7	0.2	/	/	0.2373	0.0011	11554	37	Prebble et al., 2017
OZX 518	<i>N. pachyderma</i> and <i>G. bulloides</i>	TAN1302-96	87	-0.1	0.1	19.62	0.11	/	/	13085	45	This study
OZX 519	<i>N. pachyderma</i> and <i>G. bulloides</i>	TAN1302-96	130	1.7	0.1	0.02	0.04	/	/	NDFB	/	This study
OZX 520	<i>N. pachyderma</i> and <i>G. bulloides</i>	TAN1302-96	170	-1.1	0.3	0.03	0.04	/	/	NDFB	/	This study

898

899 **Table A2:** Tie points used in construction of the TAN1302-96 age model

TAN1302-96 Depth (cm)	TAN1302-96 δ <sup>18</sup> O	LR04 Age	LR04 δ <sup>18</sup> O
110	4.710	18000	5.02
170	3.930	56000	4.35
200	3.782	70000	4.32
220	3.07	82000	3.8
230	3.23	87000	4.18
250	3.22	109000	4.12
270	2.90	123000	3.1
300	3.660	129000	3.9
320	4.350	140000	4.98

901

Formatted Table

Deleted: 260

Deleted: 3.150

Deleted: 3.71

Deleted: 115000

Deleted: 300

Deleted: 3.660

Deleted: 129000

Deleted: 3.9

Formatted Table

Deleted: 320

Deleted: 4.350

Deleted: 140000

Deleted: 4.98

Deleted: ¶

917  
918  
919  
920

**Table A3:** Sample depth and corresponding age. Diatom slides using Method 1 used sediment samples that are even (e.g., 10, 20, 30, etc.), while diatom slides using Method 2 used sediment samples that are odd (e.g., 53, 87, etc.). \* Indicates the sample was calculated based on linear sedimentation rates.

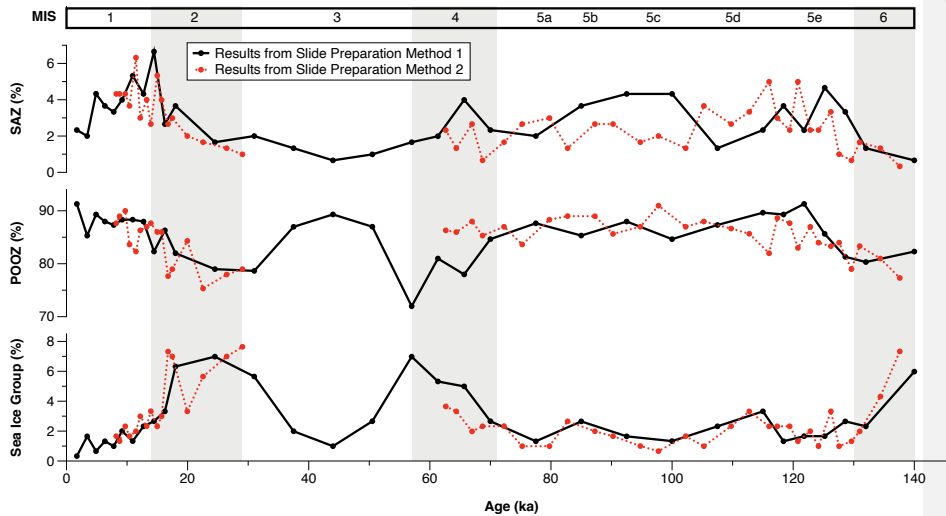
Sample Depth (cm)	Age	Sample Depth (cm)	Age	Sample Depth (cm)	Age	Sample Depth (cm)	Age
10	1001*	100	16011	197	68608	260	116007
20	2531*	103	16609	200	69999	263	118110
30	4061	107	17406	203	71790	267	120912
40	5591	110	18000	207	74196	270	123000
50	7152	113	19893	210	76000	273	123597
53	7584	117	22434	213	77802	277	124398
57	8108	120	24340	217	80207	280	124998
60	8486	123	26244	220	82000	283	125598
63	8890	127	28780	223	83491	287	126398
67	9735	130	30686	227	85503	290	126999
70	10404	140	37035	230	87000	293	127600
73	11056	150	43357	233	90289	297	128403
77	11844	160	49677	237	94703	300	129000
80	12306	170	56000	240	98011	303	130644
83	12747	180	60672	243	101314	307	132850
87	13361	183	62074	247	105715	310	134503
90	13963	187	63942	250	108999	313	136155
93	14581	190	65340	253	111094	317	138360
97	15404	193	66740	257	113903	320	140000

921

- Deleted: Age
- Deleted: Age
- Deleted: Age
- Deleted: Age
- Deleted: Sample Depth (cm)
- Deleted: Sample Depth (cm)
- Deleted: Sample Depth (cm)
- Deleted: Sample Depth (cm)
- Deleted: 114169
- Formatted Table ... [11]
- Deleted: 10
- Deleted: 1802\*
- Deleted: 100
- Deleted: 16167
- Deleted: 260
- Deleted: 197
- Deleted: 68849
- Deleted: 20
- Deleted: 3282\*
- Deleted: 103
- Deleted: 16720
- Deleted: 200
- Deleted: 70541
- Deleted: 263
- Deleted: 115690
- Deleted: 30
- Deleted: 4762
- Deleted: 107
- Deleted: 17784
- Deleted: 203
- Deleted: 72417
- Deleted: 267
- Deleted: 117398
- Deleted: 40
- Deleted: 6252
- Deleted: 110
- Deleted: 18818
- Deleted: 207
- Deleted: 75211
- Deleted: 270
- Deleted: 118536
- Deleted: 50
- Deleted: 7736
- Deleted: 113
- Deleted: 20200
- Deleted: 210
- Deleted: 77358
- Deleted: 273
- Deleted: 119565
- Deleted: 53
- Deleted: 8168
- Deleted: 117
- Deleted: 22364
- Deleted: 213
- Deleted: 79629
- Deleted: 277
- Deleted: 120909

1247

## Appendix B: Diatom Slide Preparation Comparison



Deleted: Supporting Information

Formatted: Heading 3

Deleted: ¶

Deleted: Core Name

... [3]

1248

**Figure B1:** Results from diatom slide preparation methods 1 & 2. No notable differences or biases were observed between the two different methods.

1249

1250

1251

1252

## Appendix C: TAN1302-96 and E27-23 Comparison

1253

### Potential Causes for WSIC Estimate Differences

Deleted: wSIC

1254

The third potential cause for the observed differences between TAN1302-96 and E27-23

Deleted: first

1255

WSIC estimates is through the cumulative effects of different laboratory protocols. While it is

Deleted: wSIC

1256

difficult to determine precisely how much different laboratory protocols could influence the

1257

results, we cannot exclude this explanation as a possible contributor to differences in WSIC.

Deleted: wSIC

1258

The fourth potential cause for differences in WSIC estimates between E27-23 and

Deleted: second

1259

TAN1302-96 are differences in counting and identification methods. We believe this is an

Deleted: wSIC

1260

unlikely cause for the differences observed between E27-23 and TAN1302-96 primarily because

1261

of the magnitude of counting discrepancies required to cause a difference of 50% WSIC

Deleted: wSIC

1262

estimates between the two cores. The close coupling of WSIC estimates between TAN1302-96

Deleted: wSIC

1263

and SO136-111 over the entire glacial-interglacial cycle supports that a fundamental issue

1275 relating to taxonomic identification and/or methodology is an unlikely explanation for the  
1276 observed WSIC differences.

1277 Finally, the fifth potential cause of differing WSIC estimates is selective diatom  
1278 preservation (e.g., Pichon et al., 1999; Ragueneau et al., 2000). The similarities between  
1279 TAN1302-96 and SO136-111 WSIC estimates, along with independent indicators in cores E27-23  
1280 and TAN1302-96, suggest that this is unlikely. For E27-23, Bradtmiller et al. (2009) used the  
1281 consistent relationship between  $^{231}\text{Pa}/^{230}\text{Th}$  ratios and opal fluxes to suggest that dissolution  
1282 remained relatively constant between the LGM and Holocene periods. In TAN1302-96, we  
1283 assigned a semi-quantitative diatom preservation value between 1 (extreme dissolution) and 4  
1284 (virtually perfect preservation) for each counted specimen. The average preservation of  
1285 diatoms for the entire core was  $3.38 \pm 0.13$ , with no observed bias based on sedimentation rate  
1286 or MIS. This assessment, although semi-qualitative, suggests that preservation remained  
1287 relatively constant (and good) throughout TAN1302-96, and is therefore unlikely to cause large  
1288 differences in WSIC between the two cores.

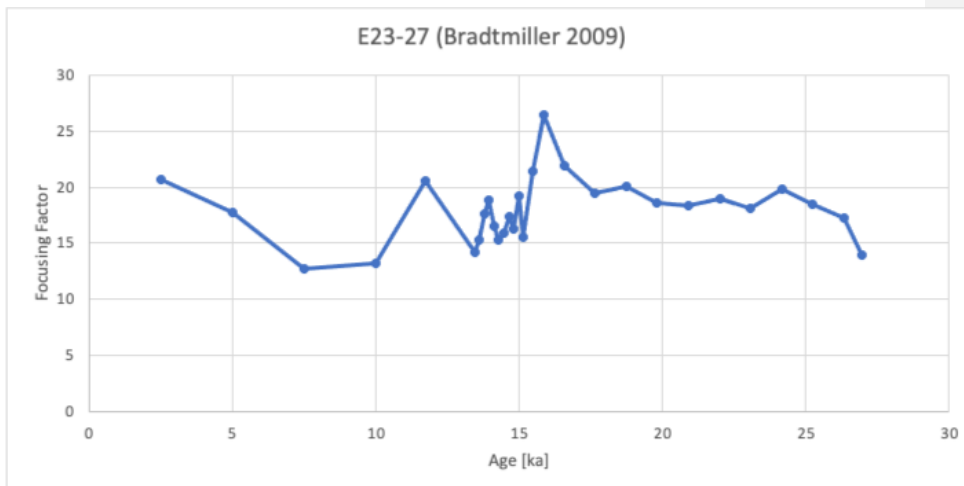
Deleted: wSIC

Deleted: ourth

Deleted: wSIC

Deleted: wSIC

Deleted: wSIC



1289 **Figure C1:** Preliminary focusing factor (FF) values for E27-23. These results suggest notable lateral sediment  
1290 redistribution over the last 26 ka BP, requiring further analysis (Bradtmiller et al., 2009).  
1291  
1292

1298 **Appendix D: %AAIW Calculation**

1299 The calculation of %AAIW in this study is the same as was used in Ronge et al. (2015):

1300  
1301 
$$\%AAIW = (\delta^{13}C_{MD97-2120} - \delta^{13}C_{MD06-2986}) / (\delta^{13}C_{MD06-2990} - \delta^{13}C_{MD06-2986}) * 100$$

1302  
1303 All core information for MD97-2120, MD06-2986, and MD06-2990, along with supporting  
1304 supplemental information can be found through the original publication.  
1305

1306 **7.0 Data Availability**

1307 All data have been published on Pangaea and can be found at:

1308 <https://doi.pangaea.de/10.1594/PANGAEA.938457>.

1309

1310 **8.0 Author Contributions**

1311 The authors confirm that the contributions to this paper are as follows: study conception and  
1312 design: KK, HB; author data collection: JJ, KK, HB, XC, ML, GD, ZC, AL; analysis and interpretation  
1313 of results: JJ, KK, HB, XC, ZC, AL, HA, GJ; draft manuscript preparation and/or editing: JJ, KK, HB,  
1314 XC, GD, ZC, AL, HA, GJ. All authors reviewed the results and approved the final version of the  
1315 manuscript.

1316

1317 **9.0 Competing Interests**

1318 The authors declare that they have no conflict of interest.

1319

1320 **10.0 Acknowledgements**

1321 This work was supported by a Canadian Natural Sciences and Engineering Research  
1322 Council grant (Discovery Grant RGPIN342251) to Karen Kohfeld. Travel funding for workshop  
1323 collaboration was provided to Jacob Jones by a Past Global Changes (PAGES) grant to the Cycles  
1324 of Sea Ice Dynamics in the Earth System (C-SIDE) Working Group. Rachel Meyne (Colgate  
1325 University) assisted with slide preparation; Maureen Soon (University of British Columbia)  
1326 assisted with opal concentration measurements; Marlow Pellatt (Parks Canada) assisted with

Deleted: s

Deleted: submitted to

Deleted: (PDI-29255) and is awaiting publication. Once Pangaea has published the dataset, the corresponding author will supply the DOI.

Deleted: ¶

1333 project conceptualization and guidance. The TAN1302-96 core was collected during the  
1334 TAN1302 RV Tangaroa voyage to the Mertz Polynya. We would like to thank the Voyage leader  
1335 Dr. Mike Williams and Captain Evan Solly and the crew, technicians and scientists involved in  
1336 the TAN1302 voyage. The voyage was co-funded by NIWA, Australian, and French research  
1337 funding. We acknowledge Dr. Andrew Kingston for running the stable isotopes at NIWA. We  
1338 acknowledge ANSTO grant AP11676 for funding the additional radiocarbon dates. This research  
1339 was partially supported by the Australian Government through the Australian Research  
1340 Council's Discovery Projects funding scheme (project DP180102357, awarded to Zanna Chase  
1341 and Helen Bostock).

1342

#### 1343 **11.0 References**

1344

1345 Abernathey, R. P., Cerovecki, I., Holland, P. R., Newsom, E., Mazloff, M., and Talley, L. D. (2016).  
1346 Water-mass transformation by sea ice in the upper branch of the Southern Ocean overturning.  
1347 *Nature Geoscience*, 9(8), 596–601. <https://doi.org/10.1038/ngeo2749>

1348

1349 Archer, D.E., Martin, P.A., Milovich, J., Brovkin, V., Plattner, G.K., and Ashendel, C. (2003).  
1350 Model sensitivity in the effect of Antarctic sea ice and stratification on atmospheric  
1351 pCO<sub>2</sub>. *Paleoceanography*, 18(1): 1012. <https://doi.org/10.1029/2002PA000760>

1352

1353 Benz, V., Esper, O., Gersonde, R., Lamy, F., and Tiedemann, R. (2016). Last Glacial Maximum sea  
1354 surface temperature and sea-ice extent in the Pacific sector of the Southern Ocean. *Quaternary  
1355 Science Reviews*, 146: 216–237. <https://doi.org/10.1016/j.quascirev.2016.06.006>

1356

1357 Bianchi, C., and Gersonde, R. (2002). The Southern Ocean surface between Marine Isotope  
1358 Stages 6 and 5d: shape and timing of climate changes. *Paleogeography, Paleoclimatology,  
1359 Paleoecology*, 187: 151–177.

1360

1361 Bereiter, B., Eggleston, S., Schmitt, J., Nehrbass-Ahles, C., Stocker, T.F., Fischer, H., Kipfstuhl, S.,  
1362 and Chappellaz, J. (2015). Revision of the EPICA Dome C CO<sub>2</sub> record from 800 to 600 kyr before  
1363 present. *Geophysical Research Letters*, 42(2): 542–549. <https://doi.org/10.1002/2014GL061957>

1364

1365 Bostock, H., Hayward, B., Neil, H., Sabaa, A., & Scott, G. (2015). Changes in the position of the  
1366 Subtropical Front south of New Zealand since the last glacial period. *Paleoceanography*, 30(7),  
1367 824–844. <https://doi.org/10.1002/2014PA002652>

1368

1369 Bouttes, N., Paillard, D., and Roche, D. M. (2010). Impact of brine-induced stratification on the  
1370 glacial carbon cycle. *Climate of the Past*, 6(5): 575–589. <https://doi.org/10.5194/cp-6-575-2010>

Formatted: Font: (Default) +Body (Calibri)

1371  
 1372 [Bouttes, N., Paillard, D., Roche, D. M., Waelbroeck, C., Kageyama, M., Laurantou, A., Michel, E.,](#)  
 1373 [and Bopp, L. \(2012\). Impact of oceanic processes on the carbon cycle during the last](#)  
 1374 [termination, \*Clim. Past\*, 8, 149–170. <https://doi.org/10.5194/cp-8-149-2012>](#)  
 1375  
 1376 Bradtmiller, L.I., Anderson, R.F., Fleisher, M.Q. and Burckle, L.H. (2009). Comparing glacial and  
 1377 Holocene opal fluxes in the Pacific sector of the Southern Ocean. *Paleoceanography*, 24(2),  
 1378 PA2214–n/a. <https://doi.org/10.1029/2008PA001693>  
 1379  
 1380 Butzin, M., Köhler, P., and Lohmann, G. (2017). Marine radiocarbon reservoir age simulations  
 1381 for the past 50,000 years. *Geophysical Research Letters*, 44(16), 8473–8480.  
 1382 <https://doi.org/10.1002/2017GL074688>  
 1383  
 1384 Butzin, M., Heaton, T.J., Köhler, P., and Lohmann, G. (2020). A short note on marine reservoir  
 1385 age simulations used in INTCAL20. *Radiocarbon*, 62(4), 1–7.  
 1386 <https://doi.org/10.1017/RDC.2020.9>  
 1387  
 1388 Cefarelli, A.O., Ferrario, M.E., Almandoz, G.O., Atencio, A.G., Akselman, R., and Vernet, M.  
 1389 (2010). Diversity of the diatom genus *Fragilariopsis* in the Argentine Sea and Antarctic waters:  
 1390 morphology, distribution and abundance. *Polar Biology*, 33(11): 1463–1484.  
 1391 <https://doi.org/10.1007/s00300-010-0794-z>  
 1392  
 1393 [Cortese, G., Dunbar, G. B., Carter, L., Scott, G., Bostock, H., Bowen, M., Crundwell, M., Hayward,](#)  
 1394 [B. W., Howard, W., Martínez, J. I., Moy, A., Neil, H., Sabaa, A., and Sturm, A. \(2013\). Southwest](#)  
 1395 [Pacific Ocean response to a warmer world: Insights from Marine Isotope Stage](#)  
 1396 [5e. \*Paleoceanography\*, 28\(3\), 585–598. <https://doi.org/10.1002/palo.20052>](#)  
 1397  
 1398 Crosta, X., Pichon, J.-J., and Burckle, L.H., (1998). Application of modern analog technique to  
 1399 marine Antarctic diatoms: reconstruction of maximum sea-ice extent at the Last Glacial  
 1400 Maximum. *Paleoceanography*, 13: 284–297.  
 1401  
 1402 Crosta, X., Sturm, A., Armand, L., and Pichon, J.-J., (2004). Late Quaternary sea ice history in the  
 1403 Indian sector of the Southern Ocean as recorded by diatom assemblages. *Marine*  
 1404 *Micropaleontology*, 50: 209–223.  
 1405  
 1406 Crosta, X., Shukla, S.K., Ther, O., Ikehara, M., Yamane, M., and Yokoyama, Y. (2020). Last  
 1407 Abundant Appearance Datum of *Hemidiscus karstenii* driven by climate change. *Marine*  
 1408 *Micropaleontology*, 157: 101861. <https://doi.org/10.1016/j.marmicro.2020.101861>  
 1409  
 1410 Delille, B., Vancoppenolle, M., Geilfus, N.X., Tilbrook, B., Lannuzel, D., Schoemann, V.,  
 1411 Becquevort, S., Carnat, G., Delille, D., Lancelot, C., Chou, L., Dieckmann, G.S., and Tison, J.L.  
 1412 (2014). Southern Ocean CO<sub>2</sub> sink: The contribution of sea ice. *Journal of Geophysical Research*,  
 1413 119(9): 6340–3655. <https://doi.org/10.1002/2014JC009941>  
 1414

Formatted: Font: (Default) +Body (Calibri), 12 pt, Font color: Text 1

Formatted: Font: (Default) +Body (Calibri), 12 pt, Font color: Text 1

Formatted: Font: (Default) +Body (Calibri), 12 pt

Formatted: Font color: Text 1



1415 Eggleston, S., and E.D. Galbraith. (2018). The devil's in the disequilibrium: multi-component  
1416 analysis of dissolved carbon and oxygen changes under a broad range of forcings in a general  
1417 circulation model. *Biogeosciences* 15: 3761-3777.  
1418  
1419 [Esper, O., Gersonde, R., and Kadagies, N. \(2010\). Diatom distribution in southeastern Pacific](#)  
1420 [surface sediments and their relationship to modern environmental variables. \*Palaeogeography,\*](#)  
1421 [\*Palaeoclimatology, Palaeoecology\*, 287\(1\), 1–27. <https://doi.org/10.1016/j.palaeo.2009.12.006>](#)  
1422  
1423 Esper, O., and Gersonde, R. (2014a). New tools for the reconstruction of Pleistocene Antarctic  
1424 Sea ice. *Palaeogeography, Paleoclimatology, Paleoecology*, 399: 260–283.  
1425 <https://doi.org/10.1016/j.palaeo.2014.01.019>  
1426  
1427 [Esper, & Gersonde, R. \(2014b\). Quaternary surface water temperature estimations: New](#)  
1428 [diatom transfer functions for the Southern Ocean. \*Palaeogeography, Palaeoclimatology,\*](#)  
1429 [\*Palaeoecology\*, 414, 1–19. <https://doi.org/10.1016/j.palaeo.2014.08.008>](#)  
1430  
1431 Fenner, J., Schrader, H., and Wienigk, H. (1976). Diatom Phytoplankton Studies in the Southern  
1432 Pacific Ocean, Composition and Correlation to the Antarctic Convergence and Its  
1433 Paleocological Significance.  
1434  
1435 Ferrari, R., Jansen, M.F., Adkins, J.F., Burke, A., Stewart, A.L., Thompson, A.F. (2014). Antarctic  
1436 sea ice control on ocean circulation in present and glacial times. *Proceedings of the National*  
1437 *Academy of Sciences of the United States of America*, 111: 8753–8758.  
1438  
1439 Ferry, A.J., Crosta, X., Quilty, P.G., Fink, D., Howard, W., and Armand, L.K. (2015). First records  
1440 of winter sea ice concentration in the southwest Pacific sector of the Southern  
1441 Ocean. *Paleoceanography*, 30(11): 1525–1539. <https://doi.org/10.1002/2014pa002764>  
1442  
1443 Froelich, P. N. (1991). Biogenic opal and carbonate accumulation rates in the Subantarctic South  
1444 Atlantic: The late Neogene of Meteor Rise site 704. *Proceedings of the Ocean Drilling Program,*  
1445 *Scientific Results*, 120, 515–549.  
1446  
1447 Fryxell, G.A., Hasle, G.R. (1976). The genus *Thalassiosira*: some species with a modified ring of  
1448 central strutted processes. *Nova Hedwigia Beihefte*, 54: 67-98.  
1449  
1450 Fryxell, G.A., Hasle, G.R., (1980). The marine diatom *Thalassiosira oestrupii*: structure,  
1451 taxonomy and distribution. *American Journal of Botany*, 67: 804-814.  
1452  
1453 Galbraith, E., and de Lavergne, C. (2019). Response of a comprehensive climate model to a  
1454 broad range of external forcings: relevance for deep ocean ventilation and the development of  
1455 late Cenozoic ice ages. *Climate Dynamics*, 52(1), 653–679. [https://doi.org/10.1007/s00382-018-](https://doi.org/10.1007/s00382-018-4157-8)  
1456 [4157-8](https://doi.org/10.1007/s00382-018-4157-8)  
1457

Formatted: Font: (Default) +Body (Calibri), 12 pt, Font color: Text 1

Formatted: Font: (Default) +Body (Calibri), Font color: Text 1

Formatted: Font: (Default) +Body (Calibri), 12 pt, Font color: Text 1

Formatted: Font: (Default) +Body (Calibri), 12 pt, Font color: Text 1

1458 Gersonde, R., and Zielinski, U. (2000). The reconstruction of late Quaternary Antarctic sea-ice  
1459 distribution—the use of diatoms as a proxy for sea-ice. *Palaeogeography, Palaeoclimatology,*  
1460 *Palaeoecology*, 162(3), 263–286. [https://doi.org/10.1016/S0031-0182\(00\)00131-0](https://doi.org/10.1016/S0031-0182(00)00131-0)  
1461  
1462 Gersonde, R., Crosta, X., Abelmann, A., and Armand, L. (2005). Sea-surface temperature and sea  
1463 ice distribution of the Southern Ocean at the EPILOG last Glacial Maximum—a circum-Antarctic  
1464 view based on siliceous microfossil records. *Quaternary Science Reviews*, 24 (7–9): 869–896.  
1465  
1466 Ghadi, P., Nair, A., Crosta, X., Mohan, R., Manoj, M.C, and Meloth, T. (2020). Antarctic sea-ice  
1467 and palaeoproductivity variation over the last 156,000 years in the Indian sector of Southern  
1468 Ocean. *Marine Micropaleontology*, 160: 101894.  
1469 <https://doi.org/10.1016/j.marmicro.2020.101894>  
1470  
1471 Govin, A., Michel, E., Labeyrie, L., Waelbroeck, C., Dewilde, F., and Jansen, E. (2009), Evidence  
1472 for northward expansion of Antarctic Bottom Water mass in the Southern Ocean during the last  
1473 glacial inception, *Paleoceanography*, 24, PA1202, doi:[10.1029/2008PA001603](https://doi.org/10.1029/2008PA001603).  
1474  
1475 Guiot, J., de Beaulieu, J.L., Chceddadi, R., David, F., Ponel, P., Reille, M. (1993). The climate of  
1476 western Europe during the last Glacial/Interglacial cycle derived from pollen and insect  
1477 remains. *Palaeogeography, Palaeoclimatology, Palaeoecology*, 103: 73–93.  
1478  
1479 Guiot, J., and de Vernal, A. (2011). Is spatial autocorrelation introducing biases in the apparent  
1480 accuracy of paleoclimatic reconstructions? *Quaternary Science Reviews*, 30(15-16): 1965–1972.  
1481 <https://doi.org/10.1016/j.quascirev.2011.04.022>  
1482  
1483 Hasle G.R., and Syvertsen, E.E. (1997) Marine diatoms. In: Tomas CR (ed) Identifying marine  
1484 phytoplankton. Academic Press, pp 5–385.  
1485  
1486 Heaton, T., Köhler, P., Butzin, M., Bard, E., Reimer, R., Austin, W., Bronk Ramsey, C., Grootes, P.,  
1487 Hughen, K., Kromer, B., Reimer, P., Adkins, J., Burke, A., Cook, M., Olsen, J., and Skinner, L.  
1488 (2020). Marine20—The Marine Radiocarbon Age Calibration Curve (0–55,000 cal  
1489 BP). *Radiocarbon*, 62(4), 779–820. <https://doi.org/10.1017/RDC.2020.68>  
1490  
1491 Johansen, J.R., and Fryxell, G.A. (1985). The genus *Thalassiosira* (Bacillariophyceae): studies on  
1492 species occurring south of the Antarctic Convergence Zone. *Deep-Sea Research. Part B.*  
1493 *Oceanographic Literature Review*, 32(12): 1050. [https://doi.org/10.1016/0198-0254\(85\)94033-6](https://doi.org/10.1016/0198-0254(85)94033-6)  
1494  
1495 Khatiwala, S, Schmittner, A, and Muglia, J. (2019). Air-sea disequilibrium enhances ocean  
1496 carbon storage during glacial periods. *Science Advances*, 5(6), eaaw4981–eaaw4981.  
1497 <https://doi.org/10.1126/sciadv.aaw4981>  
1498  
1499 Kohfeld, K.E., and Chase, Z. (2017). Temporal evolution of mechanisms controlling ocean carbon  
1500 uptake during the last glacial cycle. *Earth and Planetary Science Letters*, 472: 206–215.  
1501 <https://doi.org/10.1016/j.epsl.2017.05.015>

1502 Kohfeld, K.E., and Ridgwell, A. (2009). Glacial-Interglacial Variability in Atmospheric CO<sub>2</sub> – Surface  
 1503 Ocean-Lower Atmospheric Processes (eds C. L. Quéré and E. S. Saltzman), American  
 1504 Geophysical Union, Washington D.C.  
 1505  
 1506  
 1507 [Lhardy, F., Bouttes, N., Roche, D. M., Crosta, X., Waelbroeck, C., and Paillard, D. \(2021\) Impact](#)  
 1508 [of Southern Ocean surface conditions on deep ocean circulation during the LGM: a model](#)  
 1509 [analysis, \*Clim. Past\*, 17, 1139–1159, <https://doi.org/10.5194/cp-17-1139-2021>, 2021.](#)  
 1510  
 1511 Lisiecki, L.E., and Raymo, M.E., (2005). A Pliocene–Pleistocene stack of 57 globally dis-tributed  
 1512 benthic δ<sup>18</sup> O records. *Paleoceanography*, 20(1): 1-17. <https://doi.org/10.1029/2004PA001071>  
 1513  
 1514 Locarnini, R.A., Mishonov, A.V., Antonov, J.I., Boyer, T.P., Garcia, H.E., Baranova, O.K., Zweng,  
 1515 M.M., Paver, C.R., Reagan, J.R., Johnson, D.R., Hamilton, M., and Seidov, D. (2013). World  
 1516 Ocean atlas 2013, volume 1: Temperature. In: Levitus, S. (Ed.), A. Mishonov Technical. Vol. 73.  
 1517 pp. 40. (NOAA Atlas NESDIS).  
 1518  
 1519 Lougheed, B. C., and Obrochta, S. P. (2019). A Rapid, Deterministic Age-Depth Modeling Routine  
 1520 for Geological Sequences With Inherent Depth Uncertainty. *Paleoceanography and*  
 1521 *Paleoclimatology*, 34(1), 122–133. <https://doi.org/10.1029/2018PA003457>  
 1522  
 1523 Marzocchi, A., and Jansen, M.F. (2019). Global cooling linked to increased glacial carbon storage  
 1524 via changes in Antarctic sea ice. *Nature Geoscience*, 12(12): 1001–1005.  
 1525 <https://doi.org/10.1038/s41561-019-0466-8>  
 1526  
 1527 [Menviel, L., Joos, F., and Ritz, S. \(2012\). Simulating atmospheric CO<sub>2</sub>, 13C and the marine](#)  
 1528 [carbon cycle during the Last Glacial–Interglacial cycle: possible role for a deepening of the mean](#)  
 1529 [remineralization depth and an increase in the oceanic nutrient inventory. \*Quaternary Science\*](#)  
 1530 [Reviews, 56, 46–68. <https://doi.org/10.1016/j.quascirev.2012.09.012>.](#)  
 1531  
 1532 Mix, A.C., Bard, E., & Schneider, R. (2001). Environmental processes of the ice age: land, oceans,  
 1533 glaciers (EPILOG). *Quaternary Science Reviews*, 20(4), 627–657. [https://doi.org/10.1016/S0277-](https://doi.org/10.1016/S0277-3791(00)00145-1)  
 1534 [3791\(00\)00145-1](https://doi.org/10.1016/S0277-3791(00)00145-1)  
 1535  
 1536 Morales Maqueda, M.A., and Rahmstorf, S. (2002). Did Antarctic sea-ice expansion cause glacial  
 1537 CO<sub>2</sub> decline? *Geophysical Research Letters*, 29(1), 1011–11–3.  
 1538 <https://doi.org/10.1029/2001GL013240>  
 1539  
 1540 Oliver, K. I. C., Hoogakker, B. A. A., Crowhurst, S., Henderson, G. M., Rickaby, R. E. M., Edwards,  
 1541 N. R., and Elderfield, H. (2009). A synthesis of marine sediment core δ<sup>13</sup> C data over the last  
 1542 150 000 years. *Climate of the Past Discussions*, 5(6): 2497–2554. [https://doi.org/10.5194/cpd-5-](https://doi.org/10.5194/cpd-5-2497-2009)  
 1543 [2497-2009](https://doi.org/10.5194/cpd-5-2497-2009)  
 1544

Formatted: Font: (Default) +Body (Calibri), 12 pt, Font color: Text 1

Formatted: Font: (Default) +Body (Calibri), 12 pt, Font color: Text 1

Formatted: Font: 12 pt, Font color: Text 1

Deleted: &

Formatted: Font: (Default) +Body (Calibri), 12 pt

Formatted: Font: (Default) +Body (Calibri), 12 pt

Formatted: Font: (Default) +Body (Calibri)

1546 O'Neill, C.M., Hogg, A.M., Ellwood, M.J., Opdyke, B.N., & Eggins, S.M. (2021). Sequential  
1547 changes in ocean circulation and biological export productivity during the last glacial–  
1548 interglacial cycle: a model–data study. *Climate of the Past*, 17(1), 171–201.  
1549 <https://doi.org/10.5194/cp-17-171-2021>  
1550  
1551 Pahnke, K., Zahn, R., Elderfield, H., and Schulz, M. (2003), 340,000-year centennial-scale marine  
1552 record of Southern Hemisphere climatic oscillation, *Science*, 301: 948–952.  
1553  
1554 Pahnke, K., and Zahn, R. (2005). Southern Hemisphere Water Mass Conversion Linked with  
1555 North Atlantic Climate Variability. *Science (American Association for the Advancement of*  
1556 *Science)*, 307(5716): 1741–1746. <https://doi.org/10.1126/science.1102163>  
1557  
1558 Paterne, M., Michel, E., and Héros, V. (2019). Variability of marine 14C reservoir ages in the  
1559 Southern Ocean highlighting circulation changes between 1910 and 1950. *Earth and Planetary*  
1560 *Science Letters*, 511, 99–104. <https://doi.org/10.1016/j.epsl.2019.01.029f>  
1561  
1562 Pellichero, V., Sallée, J.B., Chapman, C., and Downes, S. (2018). The Southern Ocean meridional  
1563 overturning in the sea-ice sector is driven by freshwater fluxes. *Nature Communications*, 9(1),  
1564 1789–9. <https://doi.org/10.1038/s41467-018-04101-2>  
1565  
1566 Pichon, J.J., Bareille, G., Labracherie, M., Labeyrie, L.D., Baudrimont, A. & Turon, J.L. (1992).  
1567 Quantification of the Biogenic Silica Dissolution in Southern Ocean Sediments. *Quaternary*  
1568 *Research*, 37(3), 361–378. [https://doi.org/10.1016/0033-5894\(92\)90073-R](https://doi.org/10.1016/0033-5894(92)90073-R)  
1569  
1570 Prebble, J. G., Bostock, H. C., Cortese, G., Lorrey, A. M., Hayward, B. W., Calvo, E., Northcote, L.  
1571 C., Scott, G. H., and Neil, H. L. (2017). Evidence for a Holocene Climatic Optimum in the  
1572 southwest Pacific: A multiproxy study. *Paleoceanography*, 32(8), 763–779.  
1573 <https://doi.org/10.1002/2016PA003065>  
1574  
1575 Ragueneau, O., Tréguer, P., Leynaert, A., Anderson, R.F., Brzezinski, M.A., DeMaster, D.J.,  
1576 Dugdale, R.C., Dymond, J., Fischer, G., François, R., Heinze, C., Maier-Reimer, E., Martin-  
1577 Jézéquel, V., Nelson, D.M., & Quéguiner, B. (2000). A review of the Si cycle in the modern  
1578 ocean: recent progress and missing gaps in the application of biogenic opal as a  
1579 paleoproductivity proxy. *Global and Planetary Change*, 26(4), 317–365.  
1580 [https://doi.org/10.1016/S0921-8181\(00\)00052-7](https://doi.org/10.1016/S0921-8181(00)00052-7)  
1581  
1582 Renberg, I. (1990). A procedure for preparing large sets of diatom slides from sediment  
1583 cores. *Journal of Paleolimnology*, 4(1): 87-90. <https://doi.org/10.1007/bf00208301>  
1584  
1585 Reynolds, R., Rayner, N., Smith, T., Stokes, D., and Wang, W. (2002). An Improved In Situ and  
1586 Satellite SST Analysis for Climate. *Journal of Climate*, 15(13), 1609–1625.  
1587 [https://doi.org/10.1175/1520-0442\(2002\)015<1609:AISAS>2.0.CO;2](https://doi.org/10.1175/1520-0442(2002)015<1609:AISAS>2.0.CO;2)  
1588

Formatted: French

Formatted: English (US)

Formatted: French

1589 Reynolds, R., Smith, T., Chunying, L., Chelton, D., Casey, K., & Schlax, M. (2007). Daily High-  
1590 Resolution-Blended Analyses for Sea Surface Temperature. *Journal of Climate*, 20(22), 5473–  
1591 5496. <https://doi.org/10.1175/2007JCLI1824.1>  
1592  
1593 Ronge, T.A., Steph, S., Tiedemann, R., Prange, M., Merkel, U., Nürnberg, D., and Kuhn, G.  
1594 (2015). Pushing the boundaries: Glacial/interglacial variability of intermediate and deep waters  
1595 in the southwest Pacific over the last 350,000 years. *Paleoceanography*, 30(2): 23–38.  
1596 <https://doi.org/10.1002/2014pa002727>  
1597  
1598 Rutgers van der Loeff, M.M., Cassar, N., Nicolaus, M., Rabe, B., and Stimac, I. (2014). The  
1599 influence of sea ice cover on air-sea gas exchange estimated with radon-222 profiles. *Journal of*  
1600 *Geophysical Research, Oceans*, 119(5): 2735–2751. <https://doi.org/10.1002/2013jc009321>  
1601  
1602 Schlitzer, R. (2005). Interactive analysis and visualization of geoscience data with Ocean Data  
1603 View. *Computers and Geoscience*, 28: 1211–1218. [https://doi.org/10.1016/S0098-](https://doi.org/10.1016/S0098-3004(02)00040-7)  
1604 [3004\(02\)00040-7](https://doi.org/10.1016/S0098-3004(02)00040-7)  
1605  
1606 Schneider Mor, A., Yam, R., Bianchi, C., Kunz-Pirrung, M., Gersonde, R., & Shemesh, A. (2012).  
1607 Variable sequence of events during the past seven terminations in two deep-sea cores from the  
1608 Southern Ocean. *Quaternary Research*, 77(2), 317–325.  
1609 <https://doi.org/10.1016/j.yqres.2011.11.006>  
1610  
1611 Shin, S.I., Liu, Z., Otto-Bliesner, B., Kutzbach, J., & Vavrus, Stephen J. (2003). Southern Ocean  
1612 sea-ice control of the glacial North Atlantic thermohaline circulation. *Geophysical Research*  
1613 *Letters*, 30(2), 1096–n/a. <https://doi.org/10.1029/2002GL015513>  
1614  
1615 Sigman, D., and Boyle, E. (2000) Glacial/Interglacial variations in atmospheric carbon dioxide.  
1616 *Nature (London)*, 407(6806): 859-869. <https://doi.org/10.1038/35038000>  
1617  
1618 [Sigman, D., Fripiat, F., Studer, A. S., Kemeny, P. C., Martínez-García, A., Hain, M. P., Ai, X., Wang,](https://doi.org/10.1016/j.quascirev.2020.106732)  
1619 [X., Ren, H., and Haug, G. H. \(2021\). The Southern Ocean during the ice ages: A review of the](https://doi.org/10.1016/j.quascirev.2020.106732)  
1620 [Antarctic surface isolation hypothesis, with comparison to the North Pacific. \*Quaternary Science\*](https://doi.org/10.1016/j.quascirev.2020.106732)  
1621 [\*Reviews\*, 254, 106732. https://doi.org/10.1016/j.quascirev.2020.106732](https://doi.org/10.1016/j.quascirev.2020.106732)  
1622  
1623 Smith, R. O., Vennell, R., Bostock, H. C., & Williams, M. J. (2013). Interaction of the subtropical  
1624 front with topography around southern New Zealand. *Deep-Sea Research. Part 1,*  
1625 *Oceanographic Research Papers*, 76, 13–26. <https://doi.org/10.1016/j.dsr.2013.02.007>  
1626  
1627 Sokolov, S., & Rintoul, S. (2009). Circumpolar structure and distribution of the Antarctic  
1628 Circumpolar Current fronts: 2. Variability and relationship to sea surface height. *Journal of*  
1629 *Geophysical Research: Oceans*, 114(C11), n/a–n/a. <https://doi.org/10.1029/2008JC005248>  
1630

Formatted: Font: (Default) +Body (Calibri), 12 pt, Font color: Text 1

Formatted: Font: (Default) +Body (Calibri), Font color: Text 1

1631 Stein, K., Timmermann, A., Kwon, E.Y., and Friedrich, T. (2020). Timing and magnitude of  
1632 Southern Ocean sea ice/carbon cycle feedbacks. *Proceedings of the National Academy of*  
1633 *Sciences*, 117(9): 4498–4504. <https://doi.org/10.1073/pnas.1908670117>  
1634  
1635 Stephens, B.B., and Keeling, R.F. (2000). The influence of Antarctic sea ice on glacial–interglacial  
1636 CO2 variations. *Nature (London)*, 404(6774): 171–174. <https://doi.org/10.1038/35004556>  
1637  
1638 Studer, A. S., Sigman, D.M., Martínez-García, A., Benz, V., Winckler, G., Kuhn, G., Esper, O.,  
1639 Lamy, F., Jaccard, S.L., Wacker, L., Oleynik, S., Gersonde, R., and Haug, G.H. (2015). Antarctic  
1640 Zone nutrient conditions during the last two glacial cycles. *Paleoceanography*, 30(7): 845–862.  
1641 <https://doi.org/10.1002/2014PA002745>  
1642  
1643 Sun, X., and Matsumoto, K. (2010). Effects of sea ice on atmospheric pCO2: A revised view and  
1644 implications for glacial and future climates. *Journal of Geophysical Research:*  
1645 *Biogeosciences*, 115(G2), n/a–n/a. <https://doi.org/10.1029/2009JG001023>  
1646  
1647 Toggweiler, J. R. (1999). Variation of atmospheric CO2 by ventilation of the ocean's deepest  
1648 water. *Paleoceanography*, 14(5): 571–588. <https://doi.org/10.1029/1999PA900033>  
1649  
1650 Warnock, J.P., and Scherer, R.P. (2015). A revised method for determining the absolute  
1651 abundance of diatoms. *Journal of Paleolimnology*, 53(1): 157–163.  
1652 <https://doi.org/10.1007/s10933-014-9808-0>  
1653  
1654 Wilks, J. V., and Armand, L. K. (2017). Diversity and taxonomic identification of *Shionodiscus*  
1655 spp. in the Australian sector of the Subantarctic Zone. *Diatom Research*, 32(3): 295–307.  
1656 <https://doi.org/10.1080/0269249X.2017.1365015>  
1657  
1658 Williams, M. J. (2013). Voyage Report TAN1302, Mertz Polynya (Tech. Rep.). Wellington:  
1659 National Institute of Water and Atmospheric Research (NIWA).  
1660  
1661 Williams, T.J., Martin, E.E., Sikes, E., Starr, A., Umling, N.E., & Glaubke, R. (2021). Neodymium  
1662 isotope evidence for coupled Southern Ocean circulation and Antarctic climate throughout the  
1663 last 118,000 years. *Quaternary Science Reviews*, 260, 106915.  
1664 <https://doi.org/10.1016/j.quascirev.2021.106915>  
1665  
1666 Wilson, D.J., Piotrowski, A.M., Galy, A., and Banakar, V.K. (2015). Interhemispheric controls on  
1667 deep ocean circulation and carbon chemistry during the last two glacial cycles.  
1668 *Paleoceanography*, 30: 621–641.  
1669  
1670 Wolff, E.W., Barbante, C., Becagli, S., Bigler, M., Boutron, C.F., Castellano, E., de Angelis, M.,  
1671 Federer, U., Fischer, H., Fundel, F., Hansson, M., Hutterli, M., Jonsell, U., Karlin, T., Kaufmann,  
1672 P., Lambert, F., Littot, G.C., Mulvaney, R., Röthlisberger, R., and Wegner, A. (2010). Changes in  
1673 environment over the last 800,000 years from chemical analysis of the EPICA Dome C ice

1674 core. *Quaternary Science Reviews*, 29(1), 285–295.  
1675 <https://doi.org/10.1016/j.quascirev.2009.06.013>

Deleted: ¶

¶  
¶

Deleted: Menviel, L., Joos, F., & Ritz, S. P. (2012). Simulating atmospheric CO<sub>2</sub>, 13C and the marine carbon cycle during the Last Glacial–Interglacial cycle: possible role for a deepening of the mean remineralization depth and an increase in the oceanic nutrient inventory. *Quaternary Science Reviews*, 56, 46-68.  
<https://www.sciencedirect.com/science/article/pii/S0277379112003496>

**Page 27: [1] Formatted Table      Jacob Jones      12/9/21 3:41:00 PM**

Formatted Table

**Page 27: [2] Deleted      Jacob Jones      12/7/21 11:41:00 AM**

**Page 28: [3] Deleted      Jacob Jones      12/7/21 2:52:00 PM**